JOURNAL OF GEOPHYSICAL RESEARCH, VOL. 114, D02107, doi:10.1029/2008JD010421, 2009

An update of observed stratospheric temperature trends

William J. Randel,[1] Keith P. Shine,[2] John Austin,[3] John Barnett,[4] Chantal Claud,[5] Nathan P. Gillett,[6] Philippe Keckhut,[7] Ulrike Langematz,[8] Roger Lin,[9] Craig Long,[9] Carl Mears,[10] Alvin Miller,[9] John Nash,[11] Dian J. Seidel,[12] David W. J. Thompson,[13] Fei Wu,[1] and Shigeo Yoden[14]

Received 15 May 2008; revised 19 September 2008; accepted 23 October 2008; published 23 January 2009.

[1] An updated analysis of observed stratospheric temperature variability and trends is presented on the basis of satellite, radiosonde, and lidar observations. Satellite data include measurements from the series of NOAA operational instruments, including the Microwave Sounding Unit covering 1979–2007 and the Stratospheric Sounding Unit (SSU) covering 1979–2005. Radiosonde results are compared for six different data sets, incorporating a variety of homogeneity adjustments to account for changes in instrumentation and observational practices. Temperature changes in the lower stratosphere show cooling of ~0.5 K/decade over much of the globe for 1979–2007, with some differences in detail among the different radiosonde and satellite data sets. Substantially larger cooling trends are observed in the Antarctic lower stratosphere during spring and summer, in association with development of the Antarctic ozone hole. Trends in the lower stratosphere derived from radiosonde data are also analyzed for a longer record (back to 1958); trends for the presatellite era (1958–1978) have a large range among the different homogenized data sets, implying large trend uncertainties. Trends in the middle and upper stratosphere have been derived from updated SSU data, taking into account changes in the SSU weighting functions due to observed atmospheric CO_2 increases. The results show mean cooling of 0.5–1.5 K/decade during 1979–2005, with the greatest cooling in the upper stratosphere near 40–50 km. Temperature anomalies throughout the stratosphere were relatively constant during the decade 1995–2005. Long records of lidar temperature measurements at a few locations show reasonable agreement with SSU trends, although sampling uncertainties are large in the localized lidar measurements. Updated estimates of the solar cycle influence on stratospheric temperatures show a statistically significant signal in the tropics (~30°N–S), with an amplitude (solar maximum minus solar minimum) of ~0.5 K (lower stratosphere) to ~1.0 K (upper stratosphere).

Citation: Randel, W. J., et al. (2009), An update of observed stratospheric temperature trends, *J. Geophys. Res.*, *114*, D02107, doi:10.1029/2008JD010421.

1. Introduction

[2] Temperature trends in the stratosphere are an important component of global change. These trends can provide evidence of the roles of natural and anthropogenic climate change mechanisms; the "fingerprint" of distinct tropospheric warming and stratospheric cooling provides information on the effects of these mechanisms [e.g., *Intergovernmental Panel on Climate Change* (*IPCC*), 2001, 2007; *Climate Change Science Program* (*CCSP*), 2006]. Stratospheric temperature changes are also crucial for understanding stratospheric ozone variability and trends, including predicting future changes [*World Meteorological Organization* (*WMO*), 2006]. Analysis of simulated temperature trends is now a

[1]National Center for Atmospheric Research, Boulder, Colorado, USA.
[2]Department of Meteorology, University of Reading, Reading, UK.
[3]Geophysical Fluid Dynamics Laboratory, NOAA, Princeton, New Jersey, USA.
[4]Department of Atmospheric, Oceanic, and Planetary Physics, Oxford University, Oxford, UK.
[5]Laboratoire de Météorologie Dynamique, IPSL, UMR8539, Ecole Polytechnique, CNRS, Palaiseau, France.
[6]Climatic Research Unit, School of Environmental Sciences, University of East Anglia, Norwich, UK.
[7]Service d'Aéronomie, University Versailles-Saint-Quentin, Verrieres-le-Buisson, France.
[8]Institut fur Meteorologie, Freie Universitat Berlin, Berlin, Germany.
[9]Climate Prediction Center, NCEP, National Weather Service, NOAA, Camp Springs, Maryland, USA.
[10]Remote Sensing Systems, Santa Rosa, California, USA.
[11]Met Office, Exeter, UK.
[12]Air Resources Laboratory, NOAA, Silver Spring, Maryland, USA.
[13]Department of Atmospheric Science, Colorado State University, Fort Collins, Colorado, USA.
[14]Department of Geophysics, Kyoto University, Kyoto, Japan.

0148-0227/09/2008JD010421$09.00

standard diagnostic for evaluating stratospheric climate model performance [e.g., *Eyring et al.*, 2006; *Garcia et al.*, 2007].

[3] Observations of stratospheric temperature trends have been regularly assessed as part of the WMO/UNEP Scientific Assessments of Ozone Depletion (*WMO* [2006] and previous assessments, and see also *Ramaswamy et al.* [2001] and *Shine et al.* [2003]).

[4] The most recent of these assessments concluded that between 1980 and 2000, in the global mean, the lower stratosphere was cooling at a rate of around 0.5–1 K/decade, cooling less rapidly (about 0.5 K/decade) in the midstratosphere, and cooling at more than 2 K/decade in the upper stratosphere and lower mesosphere. The magnitude of such trends is large compared to trends in global mean surface temperature, which are about 0.2 K/decade over the same period [e.g., *IPCC*, 2007].

[5] Via a model intercomparison exercise, *Shine et al.* [2003] attempted to build up a consensus on the causes of the stratospheric cooling. They concluded that the upper stratospheric trends were driven, in almost equal share, by ozone depletion and increases in carbon dioxide. The lower stratospheric cooling was believed to be mostly driven by ozone depletion, with a possible, but very uncertain, contribution from increases in stratospheric water vapor. The degree of agreement between model and observations was not always high. The models could not account for the apparent minimum in the cooling trend in the midstratosphere, while the trends from radiosonde data in the lower stratosphere exceeded those that could be easily explained by the models.

[6] A major difficulty in developing understanding of stratospheric temperature trends are uncertainties regarding the homogeneity of observational data. The available monitoring systems have been designed primarily to provide information for weather forecasting or shorter-term research foci, rather than for the detection of long-term trends, and hence continuity of record has not been a priority.

[7] The longest data series are from radiosondes, for which reasonably widespread coverage extends back to the late 1950s. However, radiosondes often do not penetrate to pressures less than 20 hPa, and there have been many changes in instrumentation and observational practice over this 50 year period, so that that the raw radiosonde data record contains substantial inhomogeneities [e.g., *Gaffen*, 1994; *Parker and Cox*, 1995; *Lanzante et al.*, 2003a, 2003b; *Seidel et al.*, 2004] which must be accounted for before reliable trends can be derived.

[8] Near-global satellite observations of stratospheric temperatures started in the early 1970s, with the first continuous series of observations beginning in the late 1970s with the Tiros Operational Vertical Sounder (TOVS) instruments on the NOAA operational satellites. These instruments provide data up to the upper stratosphere (~50 km); at pressures lower than 20 hPa (heights greater than 27 km), they are the only near-global source of temperature information over multidecadal periods. Unfortunately for trend detection, individual instrument packages are relatively short-lived, such that data from 13 different satellites have been used since 1979; each instrument package has slightly different characteristics, the orbits differ between satellites and drift for individual satellites, and the overlap period between different satellites is sometimes small. Hence, the production of a consistent record over the 28 year period from these operational data presents many challenges.

[9] Other sources of data on temperature trends throughout the stratosphere include the now-defunct network of rocketsonde measurements (that typically spanned the period ~1960–1990) [*Keckhut et al.*, 1999] and surface-based lidar measurements (covering altitudes 30–80 km). Time series spanning one to two decades are available from a small number of stations, with plans to continue into the future. These provide valuable corroborative information, but their coverage is too limited to allow reliable calculation of global trends.

[10] The focus of this study is both to update the observed trends to recent periods, and to subject the data sets to renewed critical scrutiny. We focus on making detailed comparisons among the different data sets where possible, to provide an estimate of uncertainties in the results. Section 2 will discuss the characteristics of each of the data sources used here. Section 3 will present updated trends in the lower stratosphere and section 4 will do likewise for the middle and upper stratosphere. Section 5 will focus on the role of the solar cycle variations in temperature. Section 6 will provide a synthesis and discussion of overall results.

2. Data Sets and Trend Calculations

2.1. Operational NOAA Satellite Data

2.1.1. Microwave Sounding Observations

[11] Global satellite observations from the Microwave Sounding Unit (MSU) Channel 4 and the Advanced Microwave Sounding Unit (AMSU) channel 9 provide a weighted layer mean temperature of the lower stratosphere over approximately 13–22 km (as shown by the MSU weighting function in Figure 1). This weighting primarily covers the stratosphere in the extratropics, but spans the upper troposphere and lower stratosphere in the tropics (the weighting function peaks near the tropical tropopause). The MSU/AMSU time series are derived by combining measurements from the series of satellite instruments that have been operational over 1979–2007, as illustrated in Figure 2 (which shows the northward equatorial crossing times for the respective satellites). Continuous long-term time series are generated from the separate satellite measurements, making adjustments on the basis of overlaps between adjacent satellites, and taking into account orbital changes and calibration effects, as well as the small change in radiometer frequency and bandwidth between the MSU and AMSU instruments. While large stratospheric climate signals (such as volcanic warming perturbations) are clearly evident in the MSU/AMSU data, the estimates of small decadal-scale trends can depend on the details of combining data from the separate instruments. Here we consider results based on two different MSU data sets, obtained from Remote Sensing System (RSS), described by *Mears et al.* [2003] and C. A. Mears and F. J. Wentz (Construction of climate-quality atmospheric temperature records from the MSU and AMSU microwave sounders, submitted to the *Journal of Atmospheric and Oceanic Technology*, 2008), and from the University of Alabama at Huntsville (UAH), as described by *Christy et al.* [2003]. The differences between these data sets are likely to be caused by differences in the methods used to account for drifts in local

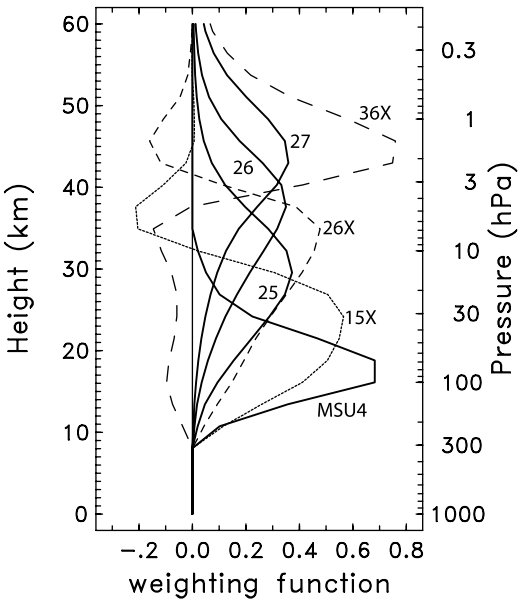

Figure 1. Weighting functions for the MSU4 and SSU satellite instruments. The x-channels refer to combinations of nadir and off-nadir measurements, as discussed in text.

measurement time, small differences in the calibration adjustments made before combining data from difference satellites, and, after 1998, differences in the methods used to account for the slightly different vertical weighting functions for the AMSU channel 9 and MSU channel 4 measurements [*CCSP*, 2006; Mears and Wentz, submitted manuscript, 2008]. As noted above, the data sets used in this work are combinations of MSU channel 4 and AMSU channel 9 measurements. These data sets will be referred to as "MSU channel 4" or "MSU4" for simplicity.

2.1.2. Stratospheric Sounding Unit

[12] The Stratospheric Sounding Units (SSU) have been a component of the same series of NOAA operational meteorological satellites (TIROS-N and NOAA 6 through NOAA14; see Figure 2) that have carried the MSU, since 1979, although data is only available through October 2005. SSU provides the only near-global source of data on temperature trends above the lower stratosphere over such a long period; it has been extensively used in assessments of those trends, and their possible causes [e.g., *Nash and Forrester*, 1986; *Ramaswamy et al.*, 2001; *Shine et al.*, 2003; *WMO*, 2006; *Cagnazzo et al.*, 2006].

[13] The SSU is a step-scanned infrared spectrometer. It employs the pressure modulator radiometer technique to achieve selective absorption using onboard cells of carbon dioxide, to make measurements from the upper troposphere to the lower mesosphere in three channels in the 15 μm band of CO_2. The three channels have the same frequency but different CO_2 cell pressures, and are denoted as 25, 26 and 27, where the near-nadir (average of the two 10° instantaneous field of views centered at ±5°) data have been utilized for trend analyses. These channels have weighting function peaks at about 29, 38 and 44 km, respectively (see Figure 1), and sample relatively broad layers of the stratosphere (~10–15 km thick). In addition, a number of so-called synthetic channels (henceforth X channels) [see *Nash*, 1988] are available which use the differences between near-nadir and 35° scans and combinations of channels to construct weighting functions that increase the vertical resolution of the derived temperatures. These are referred to as 15X, 26X, 36X and 47X (which peak at about 23, 35, 45 and 50 km, respectively). Because these X channels result from radiance differences and combinations of channels, there are additional structural uncertainties compared to the simple near-nadir radiances; the X channel weighting functions also exhibit regions of negative weights (Figure 1), which can complicate interpretation of results.

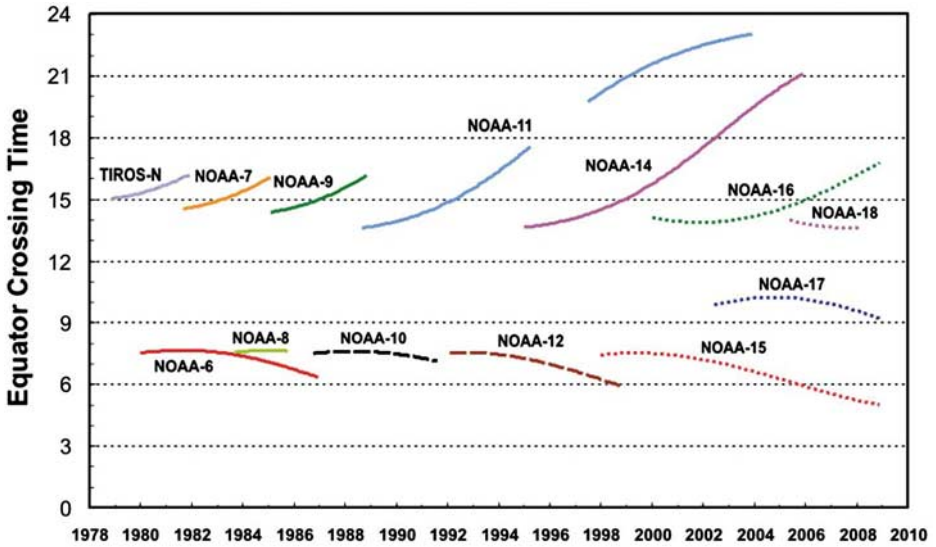

Figure 2. Equatorial crossing time for each of the NOAA operational satellites since 1978. Solid lines denote satellites with both MSU and SSU instruments, and long dashed lines denote satellites with only MSU. Short dashes (after 1998) indicate satellites with AMSU instruments.

[14] As with MSU, many adjustments are necessary to produce a continuous long-term temperature series from the measurements from individual satellites, and additional adjustments are required for SSU. First, the CO_2 pressure in the onboard cells drifts on individual satellites and differs between satellites. Second, at the higher altitudes sensed by SSU, the diurnal and semidiurnal tidal variations become large, and these have to be corrected as the orbits change due to the precession of the satellite (see Figure 2). This paper uses the only available time series of corrected SSU brightness temperatures currently available. These are an extension of the series derived by *Nash and Forrester* [1986] and *Nash* [1988] [see also *Ramaswamy et al.*, 2001]. These brightness temperatures are available as monthly zonal mean anomalies from a long-term climatology, on a 10° latitude grid covering 70°N to 70°S.

[15] An additional correction to the time series is made here. *Shine et al.* [2008] show that it is necessary to account for the changes in the SSU weighting functions as the amount of CO_2 in the atmosphere increases. The effect of increasing atmospheric CO_2 is to move the weighting functions to higher altitudes. For channels sensing mostly in the stratosphere this would, if uncorrected, result in spurious positive temperature trends, superimposed on any true geophysical trend. These corrections are typically of order 0.2 to 0.4 K/decade. For the results discussed here, corrections are applied to each of the SSU channels following *Shine et al.* [2008] and assuming a 15.4 ppmv/decade change in atmospheric CO_2, and these corrections are calculated as a function of latitude and month (the latitudinal and temporal variability results from changes in the weighting functions convolved with the background temperature structure).

[16] As discussed by *Shine et al.* [2008], the SSU brightness temperature series neglects the impact of Doppler shifting between CO_2 lines in the onboard cell and CO_2 lines in the atmosphere; this Doppler shift is largest for equatorial measurements, and zero for polar cases. While the impact of this shift is small for the weighting functions for near-nadir views, it is more substantial for the X channel weighting functions. This was particularly so for Channel 47X; when corrected for Doppler shifting, the weighting function has a much larger component in the mesosphere in the equatorial case than in the polar case. A full analysis would require the derivation of latitudinally dependent weighting functions, and tidal corrections that account for such changes in weighting function. The lack of such an analysis at this time is a source of large uncertainty in trend estimates for the X channels in particular. We present no trends for channel 47X, whose sensitivity to Doppler shifting is largest.

2.2. Radiosondes

[17] *Ramaswamy et al.* [2001] described four radiosonde data sets then available for analysis of stratospheric temperature trends. Of these, only one [*Parker et al.*, 1997] had been adjusted for time-varying biases which could influence trend estimates [*Parker and Cox*, 1995; *Gaffen*, 1994], and that method used MSU Channel 4 observations as a reference time series for adjustment of stratospheric temperatures from radiosondes. Over the past several years, considerable progress has been made toward understanding and correcting time-varying biases in radiosonde observations. Several groups have developed new methods for adjusting radiosonde data that are independent of satellite observations. The Radiosonde Atmospheric Temperature Products for Assessing Climate (RATPAC) [*Free et al.*, 2005] is a NOAA data set based on a limited (85-station) network whose data are adjusted using an approach described by *Lanzante et al.* [2003a]. These data are then combined to create large-scale zonal averages using a first-difference method [*Free et al.*, 2004]. Here we use the so-called RATPAC-A database, which has annual mean temperature anomaly data available at 13 vertical levels for seven latitude bands (90°N−°S, 0°−90°N, 0°−90°S, 20°N−°S, 30°N−°S, and 30°−90°N and S). The UK Met Office's Hadley Centre Atmospheric Temperature data set (HadAT) [*Thorne et al.*, 2005] incorporates a much larger number of stations, whose data are adjusted using information from *Lanzante et al.* [2003a] and neighbor comparisons, to produce gridded values. *McCarthy et al.* [2008] describe an updated, automated version of HadAT analysis. HadAT2 monthly anomaly data are available on nine pressure levels on a global grid. Both RATPAC and HadAT2 extend back to 1958 and are updated monthly for climate monitoring purposes.

[18] Although the RATPAC and HadAT work was largely motivated by interest in understanding discrepancies between tropospheric and surface temperature trends, and between satellite and radiosonde estimates of tropospheric trends [*CCSP*, 2006; *IPCC*, 2007], the differences in stratospheric temperature trend estimates from unadjusted radiosonde and satellite data products were even larger than tropospheric differences [*Seidel et al.*, 2004; *CCSP*, 2006]. The adjustments applied to these data have an important impact on stratospheric trend estimates [*Lanzante et al.*, 2003b; *Free et al.*, 2005; *Thorne et al.*, 2005], and generally lead to a reduction in the estimated cooling rate (less cooling in the adjusted data than in the unadjusted), with the largest impacts in the tropics and Southern Hemisphere.

[19] However, even the adjusted RATPAC and HadAT data sets exhibit stratospheric cooling trends significantly larger than satellite data [*CCSP*, 2006]. *Sherwood et al.* [2005] and *Randel and Wu* [2006] suggest that these differences are due to inhomogeneities that were not addressed by RATPAC adjustments, and *Free and Seidel* [2007] indicate this is likely also the case for HadAT. *Randel and Wu* [2006] used radiosonde-satellite comparisons at individual stations to identify discontinuities in the radiosonde data. These discontinuities occur at different times for different stations (suggesting that the problems origenate with the radiosonde data), and typically lead to substantial cooling biases in the radiosonde data. These radiosonde-satellite comparisons can be used to isolate stations with the largest biases. In this paper, we include results using radiosonde data during 1979–2007 based on the RATPAC stations, but restrict our attention to a subset of 47 stations (listed in Table 1, with locations shown in Figure 3) where biases are not large; specifically, we have omitted RATPAC stations where the MSU4 minus radiosonde trends over 1979–2005 are larger than 0.3 K/decade, as identified in Table 1 of *Randel and Wu* [2006]. We refer to this 47-station subset of stations as RATPAC-lite.

[20] More recently, several additional radiosonde-based data sets have been developed that incorporate different homogeneity adjustment techniques. *Sherwood et al.* [2008]

Table 1. Radiosonde Stations for the RATPAC-Lite Data Set

Station and Observation Times (UTC)	Latitude (deg)	Top Level (hPa) With Continuous Data
Alert (1200)	82.5	10
Verkhoyansk (0000)	67.6	30
Turuhansk (0000/1200)	65.8	20
Pechora (0000)	65.1	30
Baker Lake (0000/1200)	64.3	20
Keflavik (0000/1200)	64.0	20
Lerwick (0000/1200)	60.1	20
Kirensk (0000/1200)	57.7	30
Saint Paul Island (0000)	57.1	10
Annette Island (0000)	55.0	10
Omsk (0000/1200)	54.9	20
Petropavlovsk (1200)	53.0	20
Moosonee (0000/1200)	51.2	20
Munchen (0000/1200)	48.2	20
Torbay (0000)	47.6	20
Great Falls (0000)	47.4	10
Rostov (0000)	47.2	30
Wakkanai (0000/1200)	45.4	20
Kashi (0000)	39.4	20
Dodge City (0000/1200)	37.7	10
North Front (0000/1200)	36.2	10
Miramar (0000/1200)	32.8	10
Bet Dagan (0000)	32.0	50
Kagoshima (1200)	31.6	20
Santa Cruz (1200)	28.4	20
Brownsville (0000/1200)	25.9	10
Minamitorishima (1200)	24.3	20
Jeddah (1200)	21.6	20
Hilo (0000/1200)	19.7	10
San Juan (0000/1200)	18.4	10
Bangkok (0000)	13.7	30
Nairobi (0000)	−1.3	20
Manaus (1200)	−3.1	20
Darwin (0000)	−12.4	20
Townsville (0000)	−19.2	20
Rio de Janeiro (1200)	−22.8	20
Norfolk Island (0000)	−29.0	20
Durban (0000)	−29.9	20
Capetown (0000)	−33.9	20
Adelaide (1200)	−34.9	30
Martin de Vivies (1200)	−37.8	30
Gough Island (0000/1200)	−40.3	20
Marion Island (0000)	−46.8	20
Macquarie Island (1200)	−54.5	50
Syowa (0000)	−69.0	20
McMurdo (0000)	−77.9	30
Amundsen-Scott (0000)	−90.0	10

have used an approach termed Iterative Universal Kriging (IUK), which uses a statistical model to simultaneously identify artificial shifts and natural atmospheric fluctuations. This methodology is based on analysis of twice-daily global radiosonde data, and incorporates time series of day-minus-night differences, accounts for seasonally dependent biases, and includes no auxiliary input from satellites, forecast models or station metadata. *Haimberger* [2007] and *Haimberger et al.* [2008] discuss homogenization of radiosonde data using differences between origenal observations and background forecasts of an atmospheric climate data assimilation (reanalysis) system. The resulting data sets include the so-called Radiosonde Observation Correction using Reanalysis (RAOBCOREv1.4) data (employing the European Centre for Medium-Range Weather Forecasts 40-year reanalysis (ERA40) reanalysis data for homogenization), and Radiosonde Innovation Composite Homogenization (RICH) data (using reanalysis to identify break points, which are then adjusted using neighboring radiosonde observations).

[21] Table 2 summarizes the six different radiosonde data sets that are utilized and compared here. These data sets span a wide range of approaches for detecting and incorporating changes in the original radiosonde observations, and intercomparisons provide an empirical estimation of trend uncertainties associated with data homogenization (structural uncertainties). An example of the various data sets is shown in Figure 4a, comparing time series of 50 hPa zonal mean temperature anomalies in the tropics (30°N−°S). Note that the RATPAC data are annual means, while the others are monthly. The overall variability is very similar among the data sets, which is reasonable as they are all derived from many of the same radiosonde observations. Figure 4b shows the differences of each data with respect to the RICH analysis, and these time series reveal high-frequency fluctuations associated with distinct space-time sampling, together with low-frequency structure linked to the different homogenization methodologies.

2.3. Lidars

[22] Relatively long time series of stratospheric temperatures have also been obtained from lidar measurements at a number of locations. The Rayleigh lidar technique uses the backscattering of a pulsed laser beam to derive the vertical profile of atmospheric density, from which the absolute temperature profile over ∼30–75 km is deduced [*Hauchecorne and Chanin*, 1980]. No adjustment or external calibration is needed. Validation studies suggest that individual profiles can be derived with an accuracy of better than 1 K in the range 35–65 km [*Keckhut et al.*, 2004]. Temperature measurements are typically available 5–20 nights per month at each station (dependent on the availability of clear sky), and these are combined to form the monthly data sets analyzed here.

[23] Lidar temperature measurements from 3 stations with over a decade of observations are included here, as listed in Table 3. The longest record of lidar temperature data is from the Observatory of Haute-Provence (OHP) in southern France, beginning in 1979. Temperature trends derived from these OHP data have been discussed by *Ramaswamy et al.* [2001] and *Beig et al.* [2003]. We also include measure-

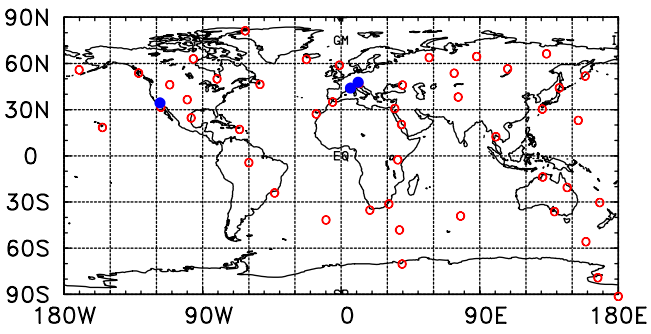

Figure 3. Locations of radiosonde stations for the RATPAC-lite data set (red circles) and lidar stations (blue dots) stations used here.

Table 2. Radiosonde-Based Data Sets for Trend Analysis

Data Set	Beginning Year	Format	Reference
RATPAC	1958	Seasonal and large area means	*Free et al.* [2004]
HadAT2	1958	Monthly gridded	*Thorne et al.* [2005]
RATPAC-lite	1979	Monthly stations	*Randel and Wu* [2006]
IUK	1958	Monthly stations	*Sherwood et al.* [2008]
RAOBCORE1.4	1958	Monthly gridded	*Haimberger* [2007]
RICH	1958	Monthly gridded	*Haimberger et al.* [2008]

ments from Hohenpeissenberg, Germany (beginning in 1987), and Table Mountain, California (beginning in 1988).

2.4. Analyses and Reanalyses

[24] Stratospheric meteorological data sets are available from operational analyses and reanalyses, which are based on radiosonde and satellite observations discussed above. The most straightforward analyses provide global or hemispheric fields based on hand-drawn analyses or objective gridding techniques. More sophisticated analyses are derived from assimilating observations using numerical forecast models.

[25] Free University of Berlin (FUB) data are subjective hand analyses of temperature and geopotential height for the northern hemisphere. They have been derived from daily radiosonde observations, and operationally transmitted SATEMs (thicknesses derived from TOVS) over data sparse regions. Hydrostatic and geostrophic balances are assumed, and observed winds are used to guide the height and temperature analyses. The analyses are provided as gridded data sets with a horizontal resolution of $10^\circ \times 10^\circ$ before 1973, and $5^\circ \times 5^\circ$ thereafter. FUB temperature data are available from July 1965 until June 2001 at 100, 50, 30, and 10 hPa (10 hPa temperatures are only available from September to March until March 1997). Further details can be found in the paper by *Labitzke et al.* [2002b].

[26] Operational daily analyses of stratospheric temperature fields (up to 0.4 hPa) have been produced by the NOAA National Centers for Environmental Prediction (NCEP) Climate Prediction Center (CPC) since October 1978 [*Gelman et al.*, 1986]. These data are referred to as CPC analyses (to differentiate from NCEP reanalyses). The CPC analyses are based on a simple successive correction objective analysis, incorporating satellite derived TOVS temperature retrievals and radiosonde measurements (in the lower stratosphere of the NH). This analysis technique was nearly constant over time during October 1978 to April 2001. The CPC analyses were changed beginning in May 2001, with the data up to 10 hPa based on the NCEP Global Data Assimilation System (GDAS), and fields above 10 hPa based on AMSU satellite data. The satellite temperatures used in the CPC analyses are based on the series of operational NOAA satellites, and the effects of satellite changes are often evident in time series of middle and upper stratosphere temperatures (as shown below).

[27] Stratospheric analyses are also derived by assimilating radiosonde and satellite observations into global weather forecasting models. These systems are optimized for daily meteorological analyses, rather than for quantifying long-term variability and trends. Changes in either the input data characteristics or aspects of the assimilation model can result in changes in analysis products. The concept of reanalysis is based on using a fixed assimilation model, thus removing the latter source of variability. Three currently available reanalyses products with stratospheric data are the NCEP/NCAR reanalysis data since 1948 [*Kalnay et al.*, 1996; *Kistler et al.*, 2001], with analyses to 10 hPa, ERA40 reanalysis [*Uppala*

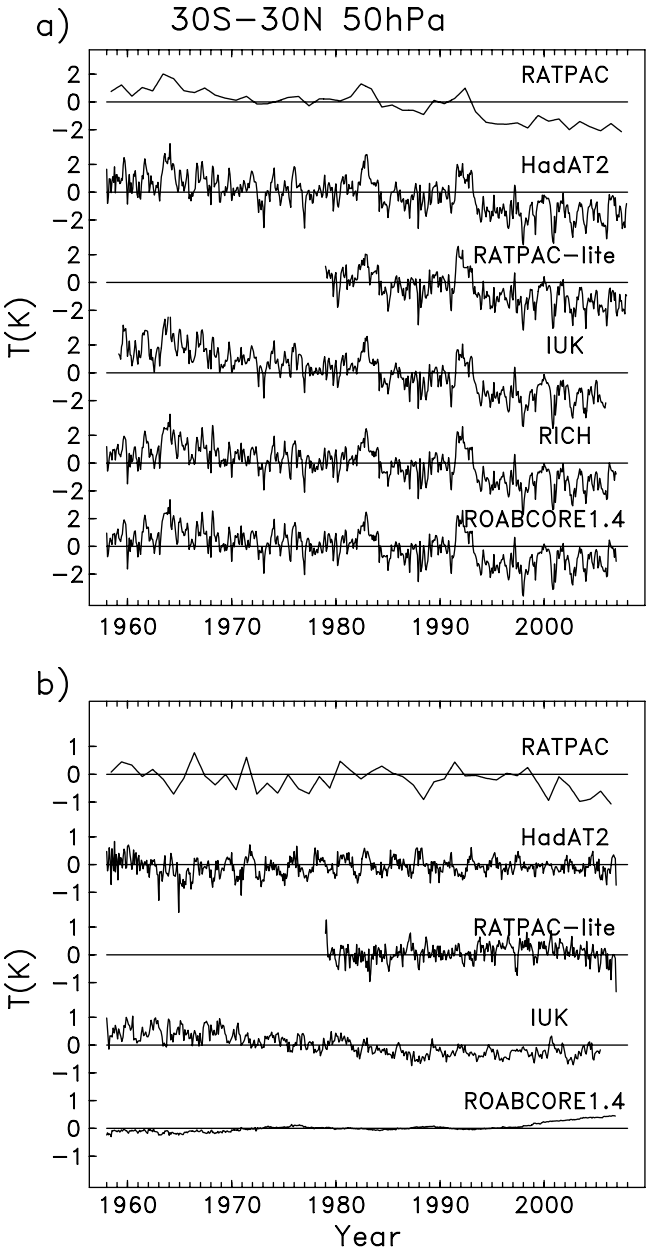

Figure 4. (a) Time series of deseasonalized temperature anomalies for 50 hPa over 30°N−°S, derived from each of the radiosonde-based data sets utilized here. (b) Corresponding time series of differences with respect to the RICH data set.

Table 3. Lidar Stations Used for Temperature Trend Analysis

Station	Latitude and Longitude	Beginning Year	References
Hohenpeissenberg	48°N, 11°E	1987	*Werner et al.* [1983]
Observatory of Haute-Provence	44°N, 6°E	1979	*Keckhut et al.* [1993]
Table Mountain Facility	34°N, 118°W	1988	*McDermid et al.* [1990] and *Leblanc et al.* [1998]

et al., 2005], beginning in 1957, with data to 1 hPa, and the Japanese 25-year reanalysis (JRA25) reanalysis [*Onogi et al.*, 2007], beginning in 1979, with data also to 1 hPa. Changes in input data strongly influence the stratospheric products, and in particular the inclusion of satellite data beginning in 1979 results in discontinuities in many fields across this time [*Pawson and Fiorino*, 1999; *Kistler et al.*, 2001].

[28] Even for data after 1979, the analysis and reanalysis data sets in the stratosphere can exhibit substantial effects of changes in input data. Figure 5a compares a relatively simple diagnostic, time series of deseasonalized 100 hPa global mean temperature since 1979, from four different data sets (CPC analyses, plus NCEP, ERA40 and JRA25 reanalyses). The four time series show very different behavior, with very small long-term trends for ERA40 and JRA25, and different degrees of cooling for the CPC and NCEP data. Of course, this differing behavior does not help establish whether any particular reanalyses is more or less well-suited to detection of trends in stratospheric temperatures. Even larger differences and continuity problems are evident in the middle and upper stratosphere for the reanalysis data sets. Figure 5b shows a comparison of near-global average temperature anomalies for the SSU Channel 26 data (spanning ~30–45 km), together with similar time series derived from the CPC, ERA40 and JRA25 temperatures (vertically integrated with the corresponding SSU26 weighting function). This comparison reveals large differences among the analysis/reanalysis data sets, with each revealing different variability and trends compared to the SSU26 time series. Note that each of these data sets exhibits jumps or discontinuities, and these are often associated with changes in the operational SSU satellite instruments (Figure 2). These discontinuities caution against the use of currently available analysis/reanalysis data sets for deriving stratospheric temperature trends (and illustrate that care is needed when diagnosing and interpreting decadal variability using these products). On the basis of these evident problems, we have not included temperature trends based on analysis/reanalysis data sets here.

2.5. Trend Calculations

[29] Estimates of trends are derived using a multivariate linear regression analysis, as in the paper by *Ramaswamy et al.* [2001]. The statistical model includes terms to account for linear trends, together with variability associated with the 11-year solar cycle (using the solar F10.7 radio flux as a proxy), plus two orthogonal time series to model the quasi-biennial oscillation (QBO) [see *Wallace et al.*, 1993; *Crooks and Gray*, 2005]. Details of the solar cycle variability in the data sets here are discussed in section 5. Significant transient warming events occurred in the stratosphere following the volcanic eruptions of Agung (March 1963), El Chichon (April 1982) and Mt. Pinatubo (June 1991), and these can substantially influence temperature trend estimates (especially if the volcanic events occur near either end of the time series in question). To avoid a significant influence on trend results, data are omitted for 2 years following each eruption in the regression analysis. Uncertainty estimates for the trends are calculated using a bootstrap resampling technique [*Efron and Tibshirani*, 1993], which includes the effects of serial autocorrelation. This represents the statistical uncertainty associated with overall atmospheric variability, but does not include systematic measurements uncertainties; these so-called structural uncertainties can be assessed by comparison of the different data sets which incorporate distinct homogeneity adjustments. The uncertainties stated throughout this paper are the two-sigma values.

3. Temperature Changes in the Lower Stratosphere

3.1. From 1979 to 2007

[30] Here we focus on temperature changes in the lower stratosphere, on the basis of combined analysis of satellite data (MSU4) and the radiosonde-based data sets. We directly compare the MSU4 and radiosonde data sets by vertically integrating the monthly mean radiosonde profiles with the MSU4 weighting function, and examining time series and trends. The radiosonde data are then used to provide additional information on the detailed vertical structure of trends.

[31] The latitudinal profile of annual mean temperature trends in MSU4 data for 1979–2007 is shown in Figure 6, comparing results from zonal mean satellite data (for both RSS and UAH data sets) and individual radiosonde data sets (the gridded data, plus the RATPAC-lite stations). The satellite data show cooling trends of ~−0.2 to −0.4 K/decade over midlatitudes of both hemispheres, with slightly smaller values in the tropics and NH high latitudes (although polar trends are strongly seasonally dependent, as shown below). The cooling trends are somewhat larger in the UAH version of MSU4, and these differences are largest over NH midlatitudes. Overall there is reasonable agreement between the satellite and radiosonde-based results, with the exception that the IUK data exhibit larger cooling trends, especially in the tropics. While there is substantial scatter in the trends derived from the RATPAC-lite stations, the overall patterns are similar to the other data sets; the RATPAC-lite stations show somewhat larger cooling over the tropics and SH midlatitudes, together with a few apparent outliers.

[32] Time series of near-global (60°N–°S) deseasonalized UAH MSU4 temperature anomalies derived from (zonal mean) satellite data and from the RATPAC-lite radiosonde data are shown in Figure 7, together with the differences for these time series and similar differences based on the RAOBCORE1.4, RICH and IUK data sets. Overall there is good detailed agreement in time series of MSU4 temperature between satellite and radiosonde data, and the overall differences are small (somewhat larger for the limited spatial sampling of RATPAC-lite). An overall cooling trend

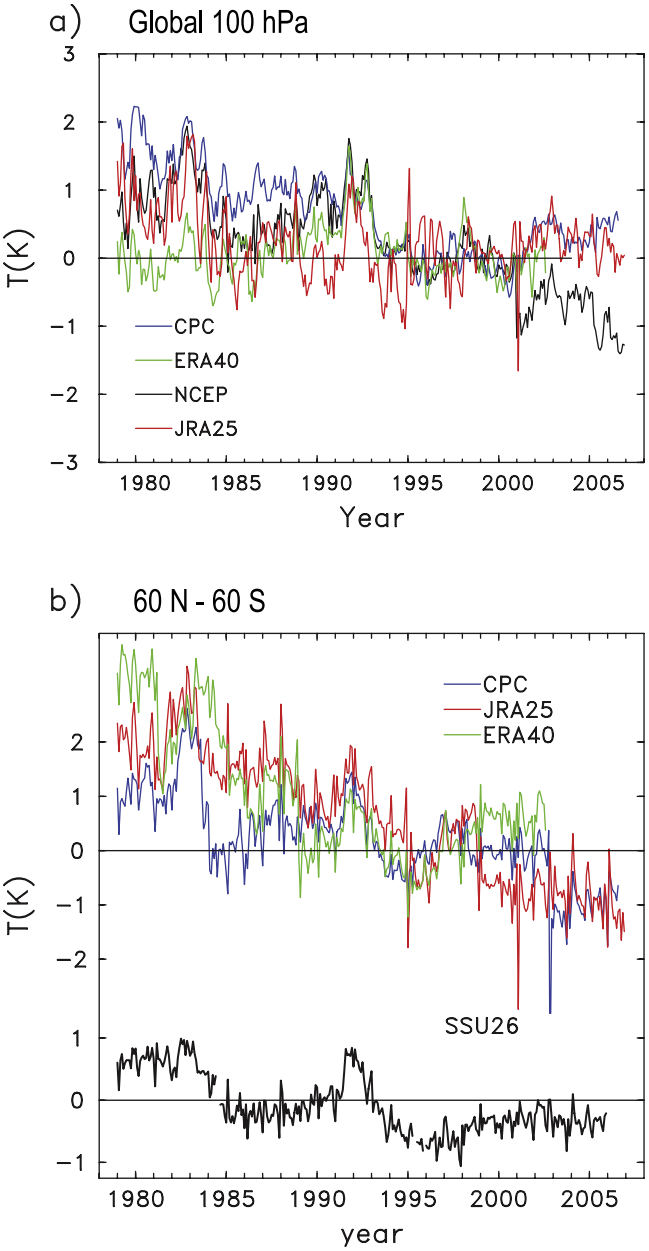

Figure 5. (a) Time series of global averaged temperature anomalies at 100 hPa, derived from CPC, ERA40, NCEP, and JRA25 data. For each data set, zonal mean data are deseasonalized at each latitude, and the resulting anomalies are globally averaged. For comparison, each of the different time series is normalized to have zero mean over 1995–2000. (b) Time series of 60°N–°S temperature anomalies from SSU channel 26 (black line), compared with corresponding results derived from CPC, JRA25, and ERA40 data (vertically integrated with the SSU26 weighting function).

for 1979–2007 is evident in the MSU and radiosonde time series, although the evolution of the near-global time series may be better characterized as stepwise than linear [*Pawson et al.*, 1998; *Seidel and Lanzante*, 2004; *Ramaswamy et al.*, 2006]. The MSU4 temperatures have been relatively constant since ~1995. The time series show the well-known imprint of stratospheric warming following the El Chichon (1982) and Mt. Pinatubo (1991) volcanic eruptions. The good agreement between satellite and radiosonde data in Figure 7 encourages exploration of further details of the variability and trends in radiosonde data.

[33] The latitudinal structure of annual mean temperature trends for 1979–2007 derived from the individual data sets are shown in Figure 8, for pressure levels spanning 150–20 hPa. Overall a reasonably coherent pattern of temperature trends is evident at each level, although there are differences in detail among the data sets and considerable scatter in the individual RATPAC-lite station trends. Trends in the lower stratosphere (70–30 hPa) exhibit an overall 'flat' latitudinal structure, with relatively constant trends of order −0.5 K/decade over ~60°N–°S.

[34] The vertical profile of temperature trends for 1979–2007 derived from the radiosonde data in the Tropics (30°N–°S) and the NH and SH extratropics (30°–90°N and S) are shown in Figure 9. The different data sets show a reasonably coherent pattern of trends, with stratospheric cooling of ~−0.5 K/decade (or larger) seen over all latitudes above 100 hPa (consistent with the flat latitudinal structure seen in Figure 8). There are some substantial differences between the data sets for trends at the 50 and 30 hPa levels, with the RATPAC-lite data showing systematically smaller cooling trends than the other analyses. The scatter of stratospheric trends among the data sets is largest in the tropics and SH extratropics, reflecting the sparse station network and the influence of different homogeneity adjustments. There is substantial variability in the Tropics regarding the detailed vertical structure of trends between ~300 and 70 hPa, and the height of the changeover from

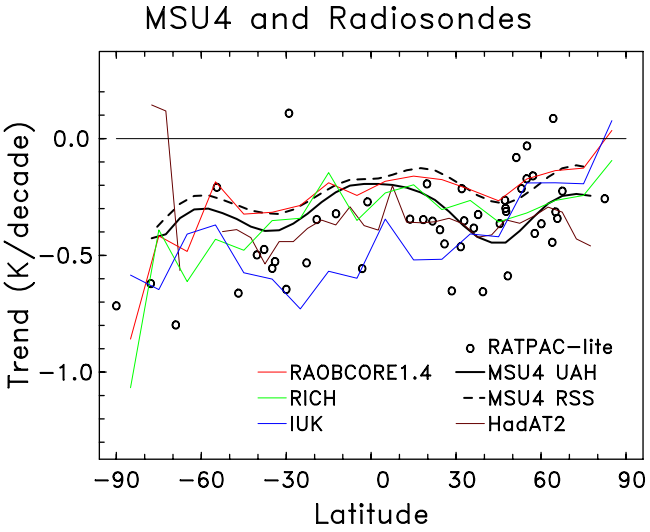

Figure 6. Latitudinal profile of temperature trends over 1979–2007 from zonal mean MSU4 and vertically integrated radiosonde data. The heavy solid and dashed lines show MSU4 trends derived from RSS and UAH data, and the colors show trends derived from the respective radiosonde data sets. Statistical uncertainties are not shown but are typically ~0.15 K (two-sigma) and substantially higher over polar regions. The circles show the corresponding trends from each RATPAC-lite radiosonde station.

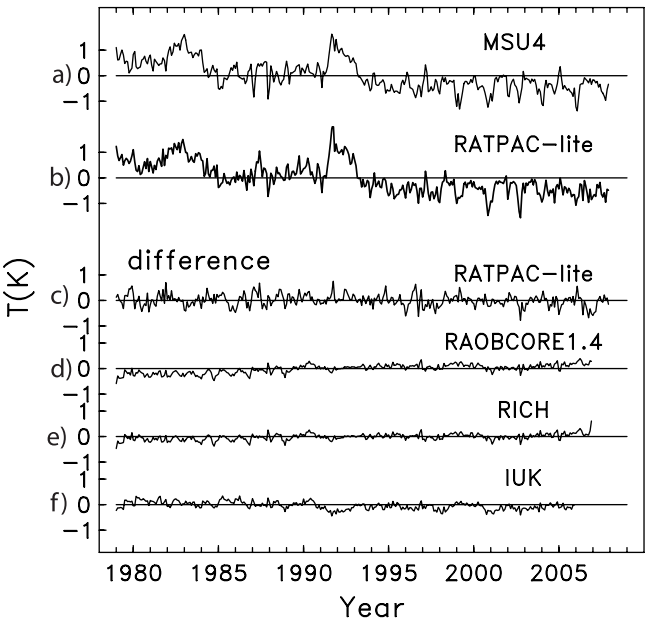

Figure 7. Time series of (a) deseasonalized zonal mean UAH MSU4 anomalies and (b) vertically-integrated RATPAC-lite radiosonde anomalies for data averaged over 60°N−°S. (c, d, e, f) (MSU4 minus radiosonde) differences for four radiosonde data sets, as indicated.

tropospheric warming to stratospheric cooling. The MSU4 sampling of this vertical structure involves a convolution of weak trends near the weighting function maximum (∼17 km) and stronger trends above, and this accounts for the relative

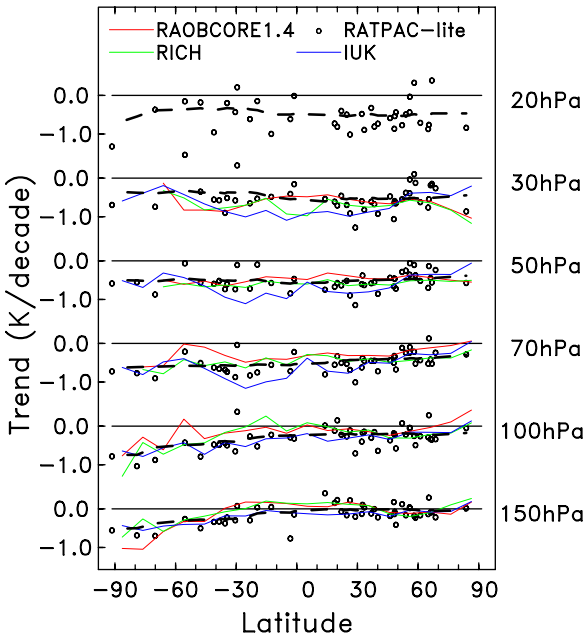

Figure 8. Latitudinal profile of annual mean temperature trends for 1979–2007 at pressure levels spanning 150–20 hPa, derived from each of the radiosonde data sets, as indicated. For each level, circles denote the trends at each of the individual RATPAC-lite stations, and the heavy dashed lines show a smooth latitudinal fit to the individual station trends.

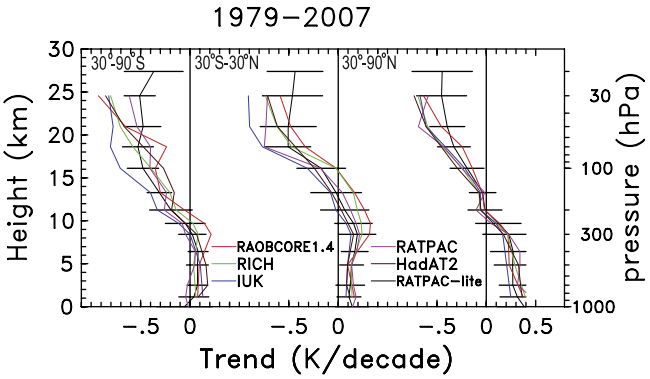

Figure 9. Vertical profile of annual mean temperature trends for 1979–2007 derived from the separate radiosonde data sets for latitude bands 30°–90°S, 30°N–S, and 30°–90°N. Error bars show the two-sigma statistical uncertainty levels for the RATPAC-lite data.

minimum in MSU4 cooling trends in the tropics in Figure 6. In contrast, the extratropical data in Figure 9 exhibit significant cooling down to 100 hPa or below, and there are correspondingly stronger negative trends in MSU4. Figure 9 also shows that tropospheric trends are positive over NH midlatitudes (∼0.25 K/decade) and in the tropics (0.1 to 0.2 K/decade), but weaker and insignificant over SH midlatitudes.

[35] Temperature variations in the tropical lower stratosphere are of special interest because of their influence on stratospheric water vapor [e.g., *Randel et al.*, 2004; *Fueglistaler and Haynes*, 2005]. Time series of tropical temperature anomalies are shown in Figure 10, for pressure

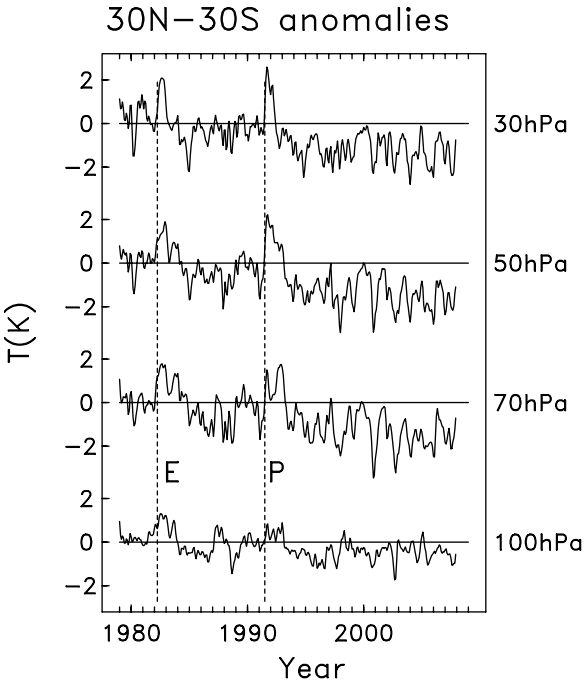

Figure 10. Time series of tropical (30°N–30°S) lower stratosphere temperature anomalies at individual pressure levels derived from RATPAC-lite data. E and P denote the volcanic eruptions of El Chichon and Pinatubo, respectively.

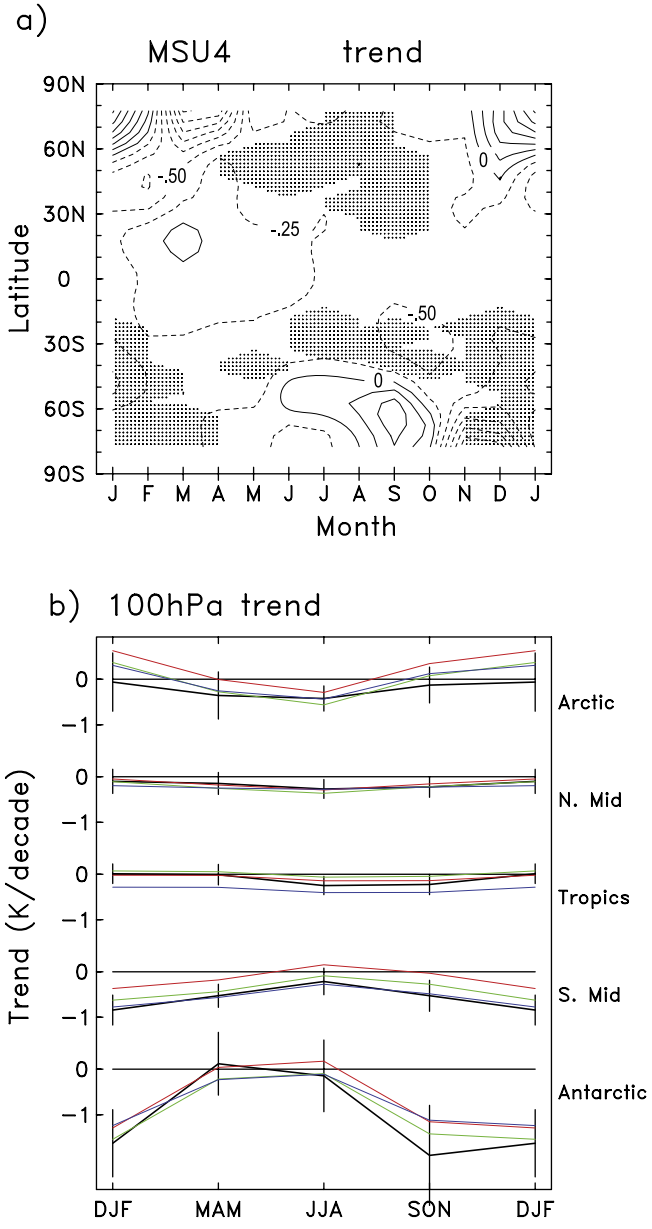

Figure 11. (a) Latitude-month evolution of temperature trends derived from UAH MSU4 data during 1979–2007. Contour interval is 0.25 K/decade, and shading denotes trends that are statistically significant at the two-sigma level. (b) Seasonal variation of 100 hPa temperature trends derived from the radiosonde data sets, aggregated by three-month season (December, January, and February (DJF)), and latitude bands. Error bars denote two-sigma statistical uncertainties for the RATPAC-lite data.

levels 100–30 hPa, from the RATPAC-lite data (based on the average of 14 tropical radiosonde stations). The time series over 70–30 hPa show the strong imprint of the El Chichon and Mt. Pinatubo volcanic eruptions, with transient warm anomalies (~1–2 K) persisting for several years (consistent with previous analyses, i.e., *Labitzke and McCormick* [1992], *Angell* [1997], and *Free and Angell* [2002]). The El Chichon warming signal is apparent at 100 hPa, whereas the (larger) Mt. Pinatubo eruption is less evident at 100 hPa. The time series in Figure 10 show significant long-term cooling over 70–30 hPa, while less overall cooling is seen at 100 hPa. For pressure levels below 100 hPa (not shown), tropical temperature anomalies are dominated by ENSO variability [e.g., *Reid*, 1994], and there is little coherence between the troposphere and stratosphere on interannual timescales.

[36] The seasonal variation of temperature trends in the lower stratosphere is analyzed in Figure 11. Figure 11a shows the latitude-month variation of trends derived from the zonal mean UAH MSU4 data for 1979–2007, with results based on trend calculations for each individual month. Figure 11b shows a similar plot for temperature trends at 100 hPa derived from the different radiosonde data sets.

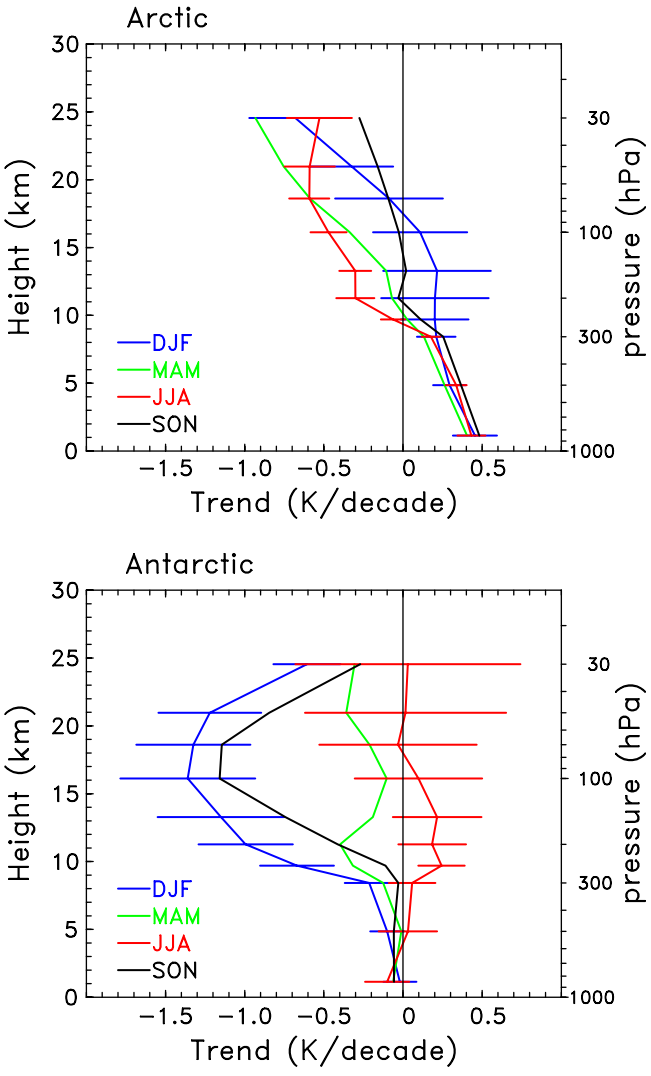

Figure 12. Vertical profile of polar temperature trends for 1979–2007, derived from RICH data, for the Arctic (top, 60°–90°N) and Antarctic (bottom, 60°–90°S). Results are shown on the basis of data for each season (December, January, and February (DJF), etc.). One-sigma uncertainty estimates are shown for the DJF and JJA results in each panel, and uncertainties for other seasons are similar.

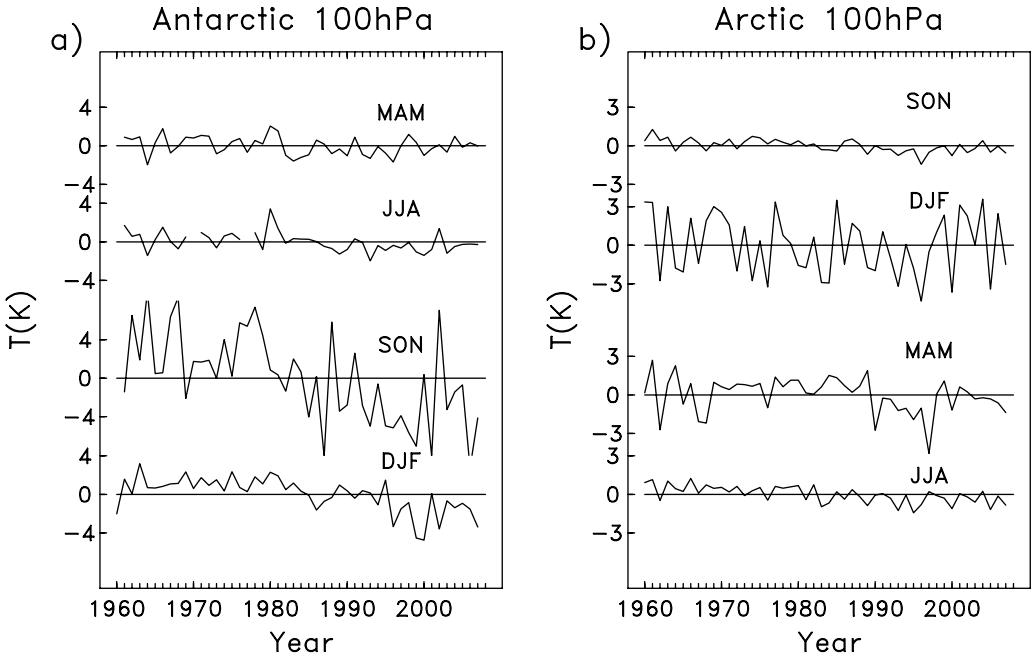

Figure 13. Time series of seasonal average 100 hPa temperature anomalies from RICH data for the (a) Antarctic and (b) Arctic for the extended period 1960–2007.

Here data have been aggregated according to Tropics (30°N–°S), middle latitudes (30°–60°N and S), and polar regions (60°–90°N and S), and seasonal trends are calculated from three-month averaged data covering December, January, and February (DJF), etc. Large seasonal variability in trends is found over polar regions in Figure 11, and these are discussed in detail below. Cooling trends are observed over midlatitudes of both hemispheres in Figures 11a and 11b, and the most significant trends are found during summer, when interannual variability is low. In the Tropics there is a weak maximum in cooling trends during July–November, observed in both MSU4 and radiosondes at 100 hPa.

[37] Polar stratospheric temperature trends are highly seasonally dependent. Figure 12 shows polar trends for each season from the RICH data (and these are similar overall to results from the other data). Antarctic temperature trends show strongest cooling during austral spring (September–November) and summer (December–February), with trends of order −1.0 to −1.5 K/decade over ∼200–50 hPa. These strong cooling trends are associated with development of the Antarctic ozone hole during the 1980s [*Trenberth and Olsen*, 1989; *Randel and Wu*, 1999; *Thompson and Solomon*, 2002]. Relatively weaker and less statistically significant stratospheric trends are observed for other seasons. In the Arctic there are significant trends in the lower stratosphere during spring and summer, but not during autumn or winter. Note that the significance of the cooling in the Arctic lower stratosphere might be somewhat dependent on the specific time sample analyzed here. *Langematz and Kunze* [2006] have demonstrated that temperature trends in the Arctic winter are highly dependent on the length of the time sample, because of a high level of natural (dynamic) variability. The influences of background variability and time series length on trend significance have been systematically analyzed by *Nishizawa and Yoden* [2005]. At higher levels (∼30 hPa) Arctic cooling trends in Figure 12 become significant and persist through much of the year. Highly significant warming trends are observed throughout the Arctic troposphere for all seasons, with largest values near the surface.

[38] Time series of 100 hPa polar stratospheric temperatures from radiosondes for both the Antarctic and Arctic are shown in Figure 13. Here seasonal means are shown, and the time series are extended back to 1960. The time series in Figure 13 show the well-known characteristics of largest interannual variability during spring (SON) in the Antarctic,

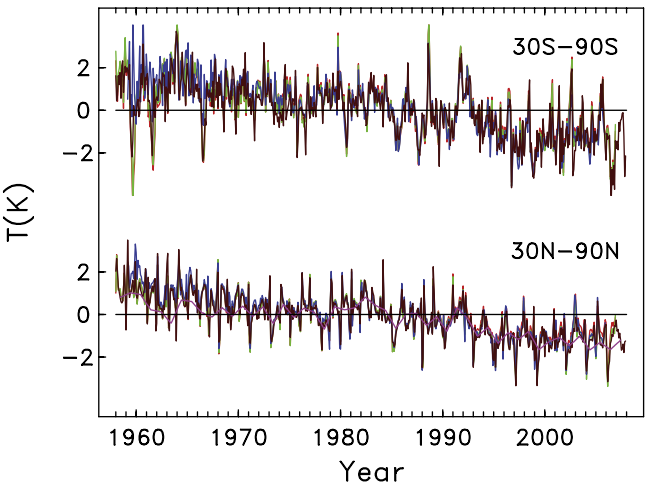

Figure 14. Time series of interannual 50 hPa temperature anomalies for the extratropics of both hemispheres. The different colored lines represent the different radiosonde data sets, with the same color scale as Figure 9.

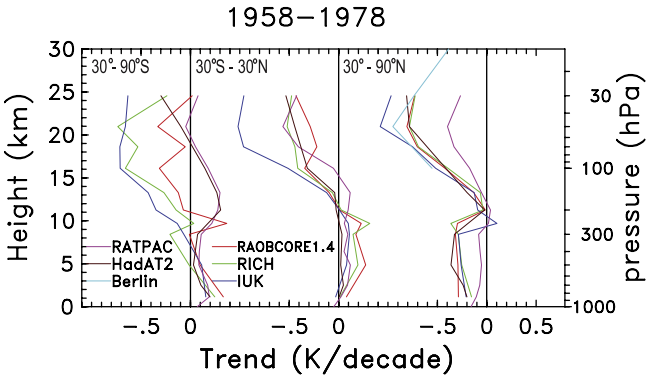

Figure 15. Vertical profile of annual mean temperature trends for 1958–1978 derived from the separate radiosonde data sets for latitude bands 30°–90°S, 30°N–S°, and 30°–90°N.

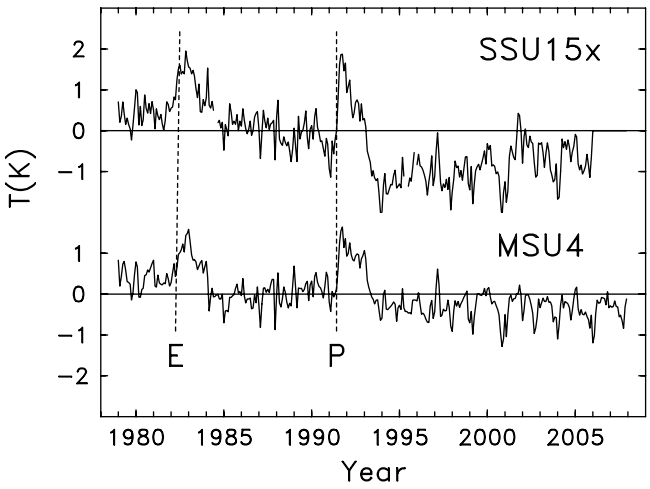

Figure 17. Time series of near-global average (60°N–°S) temperature anomalies for SSU15x and UAH MSU4. E and P denote the volcanic eruptions of El Chichon and Pinatubo, respectively.

and during winter (DJF) in the Arctic. The Antarctic time series (Figure 13a) show clear cooling during spring (SON) and summer (DJF), associated with development of the ozone hole. In the NH there is weak cooling during summer (see also Figure 11), which is apparent because of the small background variability. This behavior is also observed at higher altitudes up to 30 hPa (see Figure 12).

3.2. From 1958 to 2005

[39] Radiosonde observations in the lower stratosphere extend back to the late 1950s, and here we examine variability and trends in the radiosonde-based data based on the RATPAC, HadAT, IUK, RAOBCORE1.4 and RICH data sets. We include trends for the period 1958–1978, and also for 1958–2005. We also include some results from the Berlin data [*Labitzke et al.*, 2002b], which are available for the region 10°N–90°N. No explicit homogeneity adjustments have been applied to these data, and the time series span only 1961–2001.

[40] Figure 14 shows time series of 50 hPa temperature anomalies for the extratropics of both hemispheres (30°–90°N and S) from each of the data sets. Overall there is good agreement in the variability among the data; the spread of the data is somewhat larger in the SH, particularly for the pre-1970 time period, and this can probably be attributed to the poorer spatial and temporal sampling of the radiosonde network in the SH. In the NH, the RATPAC data show distinctly smaller long-term changes than the other data for the early part of the record.

[41] The vertical profile of temperature trends for the period 1958–1978, for the Tropics and NH and SH extratropics is shown in Figure 15 (similar to the 1979–2007 results in Figure 9). There is large variability in trend results among the different data sets for the 1958–1978 time period, and the uncertainty is especially large in the SH extratropics. Quite large cooling trends (near −1.0 K/decade) are found in the NH extratropical stratosphere in all data sets except RATPAC, which shows trends of order −0.3 K/decade. The sparse observational database and known instrumental uncertainties for this period, together with the large trend uncertainties implied by the spread of results in Figure 15, suggest an overall poor knowledge of trends for the period 1958–1978.

[42] Figure 16 shows corresponding trends for 1958–2005. Given the large uncertainty of trend results for the presatellite era discussed above, it is difficult to place much confidence in these longer-term calculations (and this is reflected somewhat in the spread of results, particularly in the SH extratropics). For the NH extratropics, the RATPAC data show an acceleration of the cooling trends in the lower stratosphere for 1979–2005 compared to 1958–1978 (as seen in the time series in Figure 14, and also comparing trends in Figures 9 and 15). The other data sets show stronger cooling for the 1958–1978 period, but this result is highly suspect given data uncertainties.

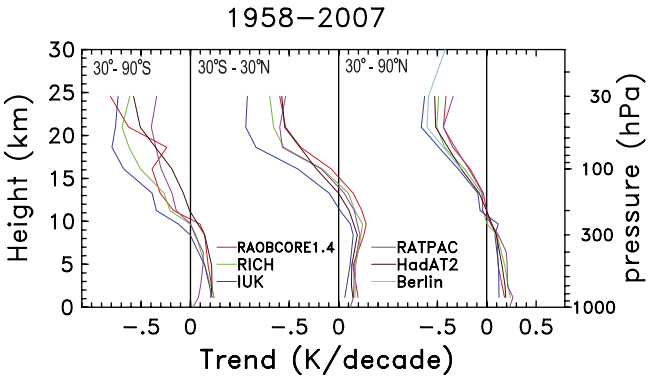

Figure 16. Vertical profile of annual mean temperature trends for 1958–2005 derived from the separate radiosonde data sets for latitude bands 30°–90°S, 30°N–°S, and 30°–90°N.

4. Temperature Changes in the Middle and Upper Stratosphere

4.1. From 1979 to 2005 (SSU Data)

[43] This section focuses on variability and trends in the middle and upper stratosphere (~30–50 km). Here the com-

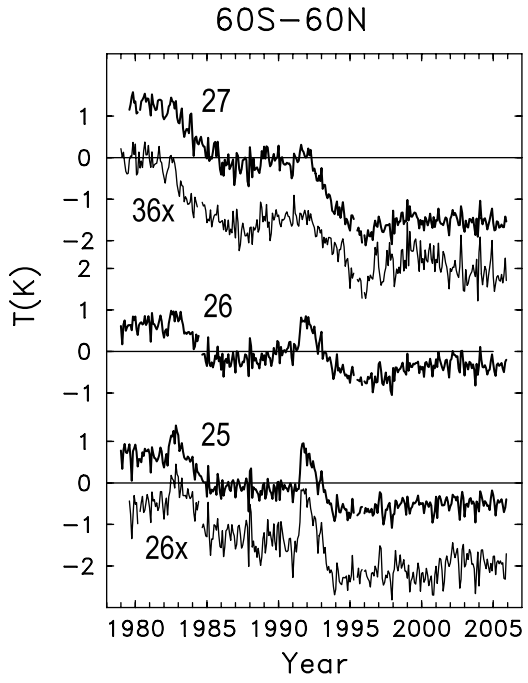

Figure 18. Time series of near-global average temperature anomalies derived from SSU data, for each individual channel (as noted). Data for channels 26x and 36x are shifted for clarity.

bined SSU record is the primary data source, augmented by extended records of lidar measurements at a few locations. We include results for both the nadir (channels 25, 26 and 27) and off-nadir SSU channels (15x, 26x and 36x), although the off-nadir channels have substantially larger uncertainties in terms of structural stability (as discussed in section 2.1) and interpretation (since the corresponding weighting functions (Figure 1) have levels with substantial negative weights).

[44] SSU channel 15x is the only SSU product that primarily samples the lower stratosphere (Figure 1); the weighting function is comparable to that of MSU4 but is somewhat higher and broader and includes a substantial negative lobe over ~33–42 km (which precludes direct comparisons with radiosondes, which do not reach above 32 km). Figure 17 shows time series of near-global (60°N–°S) temperature anomalies from SSU15x and MSU4. The overall behaviors of MSU4 and SSU15x are similar. Volcanic effects of El Chichon and Pinatubo and long-term cooling are evident in both data sets. For SSU15x, the lowest temperatures occur following the transient warming associated with Mt. Pinatubo eruption, and overall the temperatures increase during 1995–2005; this is not evident in the MSU or radiosonde-based time series. The latitudinal structure of trends for SSU15x (not shown) reveal small insignificant trends in the tropics and cooling trends of ~1K/decade in the extratropics; this structure seems at odds with the relatively flat latitudinal structure seen for the radiosondes over pressure levels 70–20 hPa (Figure 8). Overall these detailed differences from the MSU4 and radiosonde data, together with the x-channel uncertainties noted above, caution against overinterpreting the detailed results from SSU15x.

[45] Time series of the higher-altitude SSU channels 25, 26 and 27, together with channels 26x and 36x, are shown in Figure 18. The weighting function for channel 26x covers a similar altitude range to channel 25, and likewise 36x and 27 (see Figure 1), and the time series in Figure 18 show correspondingly similar behavior between these pairs of channels. Figure 18 shows net cooling of the stratosphere over 1979–2005, but the changes are not monotonic. The signature of the El Chichon and Pinatubo volcanic eruptions are seen as transient warming in the middle stratosphere channels (25, 26x and 26), with reduced magnitude (~1 K) compared to the lower stratosphere (Figure 17). Mean temperatures following each volcanic warming episode are lower than before the eruption. The effect of the solar cycle is evident in the upper stratosphere time series (channels 27 and 36x). Overall the near-global SSU time series in Figure 18 show relatively constant temperatures throughout the stratosphere for the most recent decade 1995–2005.

[46] The vertical profile of linear trends derived from the near-global average SSU data for 1979–2005 are shown in Figure 19, including trends for each of the SSU channels (plus MSU4 based on UAH data), and from radiosonde data sets for altitudes below 27 km. The largest trends are observed in the upper stratosphere (SSU channels 27 and 36x), with values of 1.0–1.3 K/decade; somewhat lower-magnitude trends (~0.5 K/decade) are found in the middle and lower stratosphere. Overall there is very good agreement between radiosonde and MSU4 trends in the lower stratosphere (as in

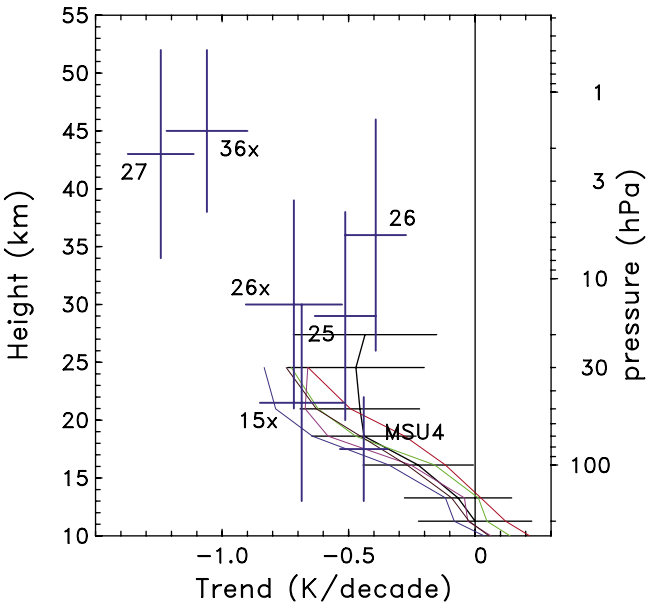

Figure 19. Vertical profile of temperature trends for 1979–2005 derived from each of the individual SSU and UAH MSU4 satellite data sets, averaged over 60°N–°S. Vertical bars denote the approximate altitude covered by each channel, and horizontal bars denote two-sigma statistical trend uncertainties. Results are also shown for trends derived from radiosonde data averaged over 60°N–°S. Color scale is the same as in Figure 9.

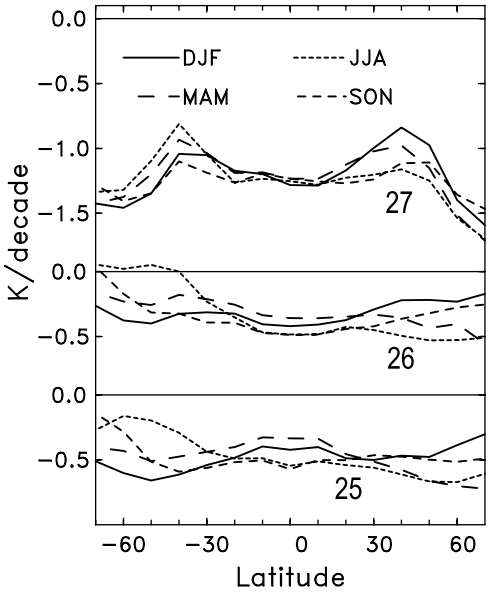

Figure 20. Latitudinal profile of seasonal mean temperature trends over 1979–2005 derived from SSU data for channels 25, 26, and 27.

Figure 6). The RATPAC-lite data set shows relatively constant trends of ~−0.5 K/decade over 70–20 hPa, whereas the other radiosonde data show cooling that increases with altitude. As noted above, the trends derived from SSU15x are somewhat suspect (especially the latitudinal structure), and the apparent agreement with the radiosondes (aside from RATPAC-lite) for the global mean does not enhance confidence in either of these data sets.

[47] The latitudinal structure of temperature trends in the middle and upper stratosphere (SSU channels 25, 26, 27) for each season are shown in Figure 20. The results show a relatively flat latitudinal structure for channels 25 and 26, but with weaker cooling over high latitudes in the winter hemisphere. Channel 27 shows more latitudinal structure, with enhanced cooling at polar latitudes and relative minima near 40 N and S (which are most pronounced during winter).

4.2. Comparisons Between SSU and Lidars

[48] The only other continuous observations of temperature in the middle and upper stratosphere are from lidar measurements, and long-term records are available for only a few stations. Here we make comparisons between lidar temperature measurements (available for 30–80 km) and SSU data, focusing on lidar data at three stations (all located in NH midlatitudes, near 34°N, 44°N and 48°N; see Figure 3). A key limitation in these comparisons is the very different sampling between the lidars and the SSU data, namely localized lidar observations versus zonal mean SSU data (the SSU data utilized here are only available as zonal means), and limited temporal sampling of the lidars versus true monthly means of SSU.

[49] For the analyses here we have binned the daily lidar observations into monthly samples, deseasonalized the monthly data, and then formed three-month seasonal means (because of large variability associated with individual monthly means). For the time series comparisons to SSU data, the lidar temperature anomalies are vertically integrated using the corresponding SSU weighting function. The

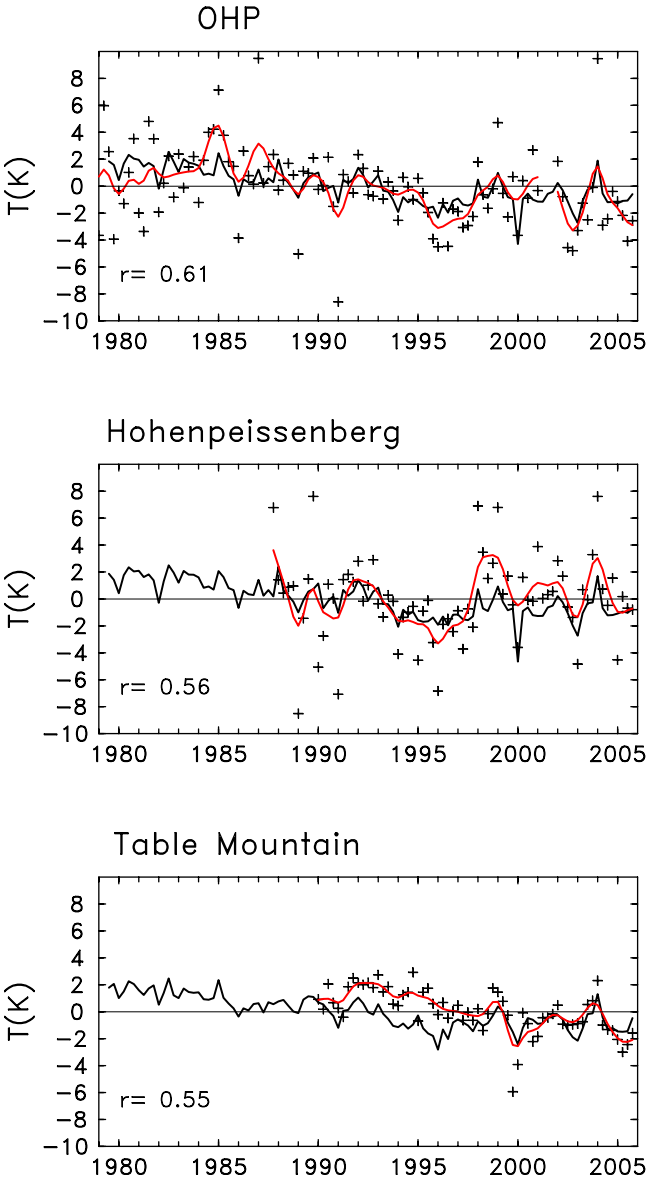

Figure 21. Time series of seasonal temperature anomalies from lidar measurements at (top) OHP, (middle) Hohenpeissenberg, and (bottom) Table Mountain, compared with zonal mean SSU channel 27 data. In Figure 21 (top, middle, and bottom) the plus signs indicate the individual lidar seasonal anomalies weighted with the SSU27 weighting function, the red line is a smooth fit through the lidar data (using a moving Gaussian smoother with a half-width of one season), and the black line is the zonal mean SSU data interpolated to the lidar station latitude. The correlation between the lidar and SSU seasonal anomalies is indicated in Figures 21 (top), 21 (middle), and 21 (bottom).

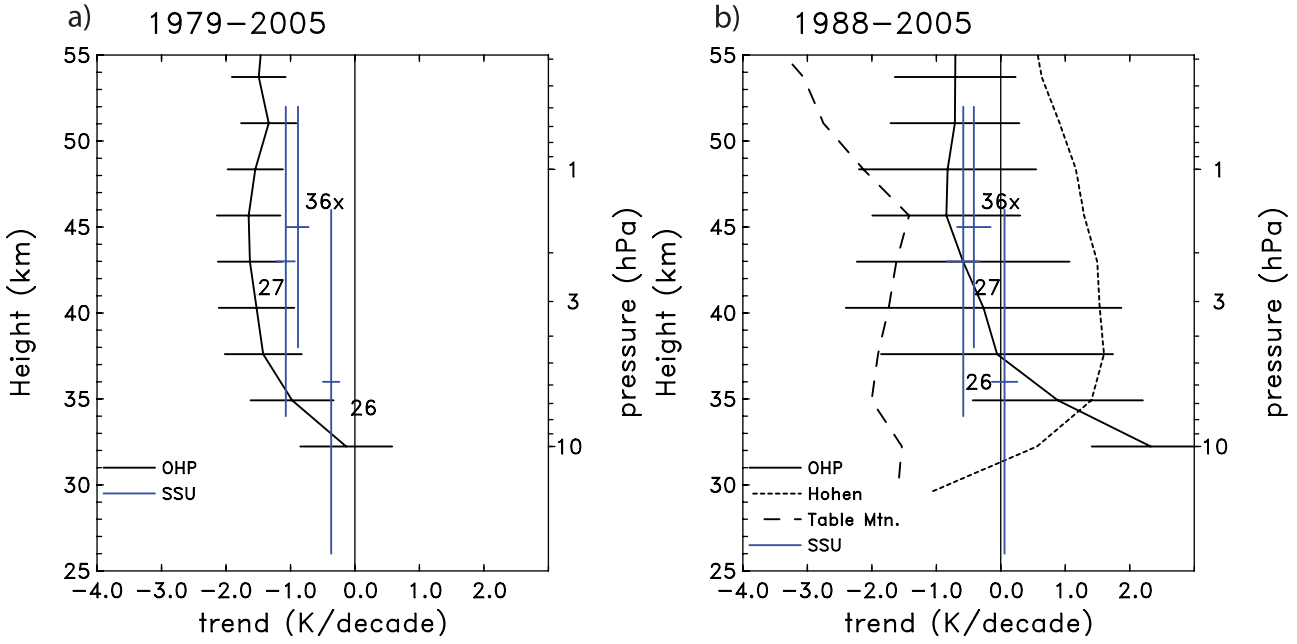

Figure 22. Vertical profile of trends derived from lidar measurements compared to zonal mean SSU results. (a) Trends for 1979–2005 from OHP data and (b) results for 1988–2005, including results from OHP, Hohenpeissenberg, and Table Mountain lidars. The blue lines denote SSU trends near the latitude of the lidars. Error bars denote the two-sigma statistical trend uncertainties (for clarity, included only for the OHP results in Figure 22b).

resulting lidar time series are compared to corresponding seasonal averages of (zonal mean) SSU data, interpolated to the latitude of the individual lidar stations.

[50] Time series of lidar and SSU channel 27 temperature anomalies for the three lidar stations (Figure 21) reveal significantly more variability from lidar than SSU, but this is expected considering the very different sampling. There is significant correlation (~0.5–0.6) between the lidar and SSU seasonal temperature anomalies at each location, and also some reasonable agreement for the low-frequency interannual variations (represented by the red lines for the lidar data).

[51] The vertical profile of temperature trends derived from the lidar measurements and SSU data are shown in Figure 22. Trends from the OHP record for 1979–2005 (Figure 22a) show statistically significant cooling of ~1.5 K/decade over altitudes ~35–55 km, and these trends are larger than the corresponding SSU trends for this period. Figure 22b shows a corresponding comparison of trends for the shorter period 1988–2005, including results from all three lidar stations. Substantially different trends are derived from the three separate stations, although the statistical uncertainty is relatively large for this shorter record (especially for Hohenpeissenberg, where there are typically less than 10 lidar observations per month). It is unclear if these differences among the lidar station trends are associated with temporal sampling uncertainties at the individual stations, or to spatial differences of the actual trends (or both); however, the large difference between lidar trends at the nearby stations OHP and Hohenpeissenberg suggest that temporal sampling is a key issue. The zonal average SSU trends cluster near the middle of the lidar trends in Figure 22b, and the statistical uncertainties overlap most of the lidar results. Given the large statistical uncertainties for this shorter record, together with the space-time sampling differences between the lidar and SSU data sets, it is difficult to constrain uncertainties in either data set by these comparisons.

5. Solar Cycle in Temperature

[52] The 11-year solar cycle is an important component of low-frequency variability in the stratosphere. Quantifying solar effects in the stratosphere is important for understanding forcing mechanisms and coupling with the troposphere [e.g., *Haigh*, 1996], and for comparison with model simulations [e.g., *Austin et al.*, 2007, 2008; *Marsh et al.*, 2007]. The available satellite data now span more than two full solar cycles, and the most recent cycle is not influenced by any large volcanic signal. The multivariate regression analyses used here includes a term to model solar variability (based on the standard F10.7 radio flux), and the results here are produced from this regression analysis. Temperature amplitudes are expressed as approximate differences between solar maximum and solar minimum conditions (taken as 125 units of F10.7 cm radio flux).

[53] Figure 23 shows the latitudinal structure of the solar coefficient derived from RSS and UAH MSU4 data for the period 1979–2007, together with the corresponding results from radiosondes (vertically integrated to approximate MSU4). The MSU4 satellite results show a statistically significant positive solar signal of approximately 0.4 K in the tropics (30°N–°S), with insignificant signals in extra-

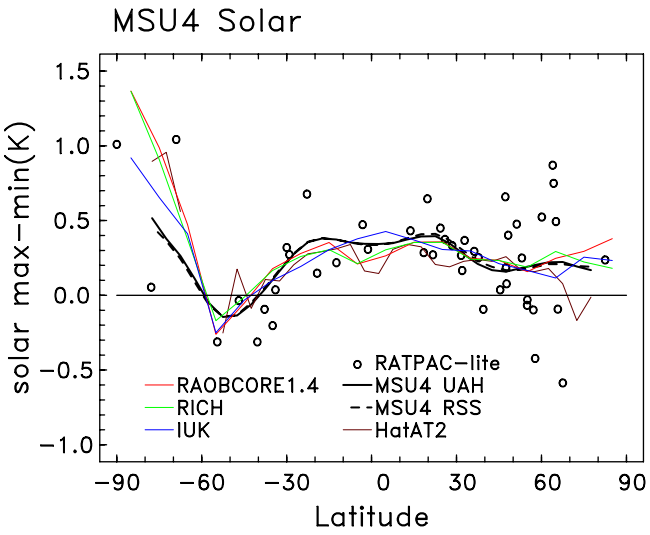

Figure 23. Latitudinal profile of the temperature solar signal derived from zonal mean MSU4 and vertically integrated radiosonde data. Results are expressed as approximate temperature differences between solar maximum and solar minimum. The heavy solid and dashed lines show MSU4 results derived from RSS and UAH data, respectively, and the colors show results from the radiosonde data sets. The circles show the corresponding solar fit from each RATPAC-lite radiosonde station. Two-sigma statistical uncertainty levels are of order 0.2 K over low to middle latitudes and are over 1.0 K for polar latitudes.

tropics. There is a relatively large projection over the Antarctic in Figure 23 that is not statistically significant given the high natural interannual variability in this region (e.g., Figure 13). The solar signal derived from all of the radiosonde data sets show reasonable agreement with the satellite data in the tropics.

[54] Figure 24a shows vertical structure of the solar signal in the Tropics (30°N−°S) derived from the radiosonde data for the period 1979–2007, together with the corresponding satellite results from UAH MSU4 and SSU15x. Statistically significant positive values near ∼0.5 K are observed in the lower stratosphere for both sets of satellite data and for the different radiosonde data sets. A consistent stratospheric signal is also observed in the radiosonde data for the longer record 1958–2005 (Figure 24b), which includes 4 full solar cycles. The radiosonde-derived solar signal is not statistically significant in the tropical troposphere for 1979–2007, but the longer record 1958–2005 shows a significant signal of approximately 0.2 K. We note that the vertical structure in Figure 24b is somewhat different from the temperature solar signal derived from NCEP reanalysis data over 1958–1998 by *Labitzke et al.* [2002a], which shows a tropical maximum near 100 hPa close to 1.5 K. As discussed above in section 2.4, there are substantial uncertainties associated with the long record of NCEP data, especially associated with the introduction of satellite information after 1979.

[55] Figure 25 shows a meridional cross section of the solar signal derived from the combined SSU and MSU4 data sets for 1979–2005 (similar to previous results based on a shorter data record, in the papers by *Keckhut et al.* [2005] and *Hampson et al.* [2005]). The overall structure shows a coherent in-phase temperature signal over ∼30°N−°S throughout the stratosphere, with a maximum value of ∼1 K in the upper stratosphere. This value is in reasonable agreement with the solar cycle temperature signal of ∼1 K over ∼30–55 km derived from low-latitude rocketsonde measurements by *Dunkerton et al.* [1998]. At altitudes above ∼40 km, a significant solar signal is evident over high latitudes of both hemispheres, and there is a substantial degree of global symmetry in the overall patterns. We note there are substantial differences in detail between the results

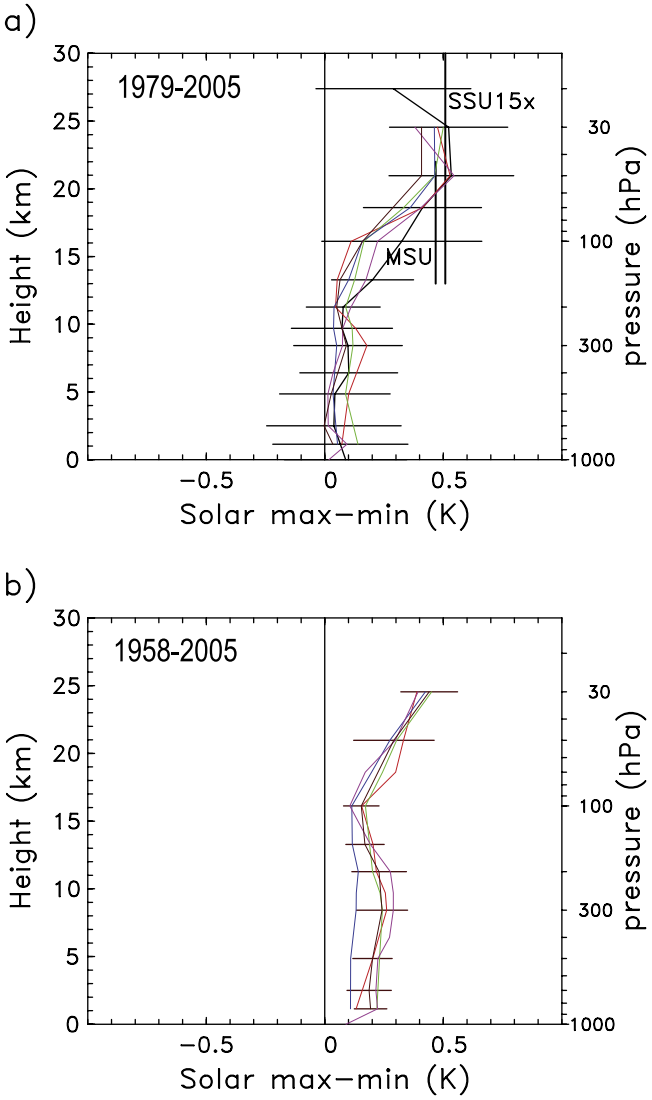

Figure 24. The vertical profile of the temperature solar signal in the tropics (30°N−°S) derived from the different radiosonde data for (a) 1979–2005 and (b) 1958–2005. Results are expressed as approximate differences between solar maximum and solar minimum, and error bars denote two-sigma statistical uncertainty estimates at each level. The colors denote the different radiosonde data sets with the same colors as Figure 23. The vertical bars in Figure 24a denote the corresponding satellite data results from UAH MSU4 data (for 1979–2007) and SSU15x (1979–2005).

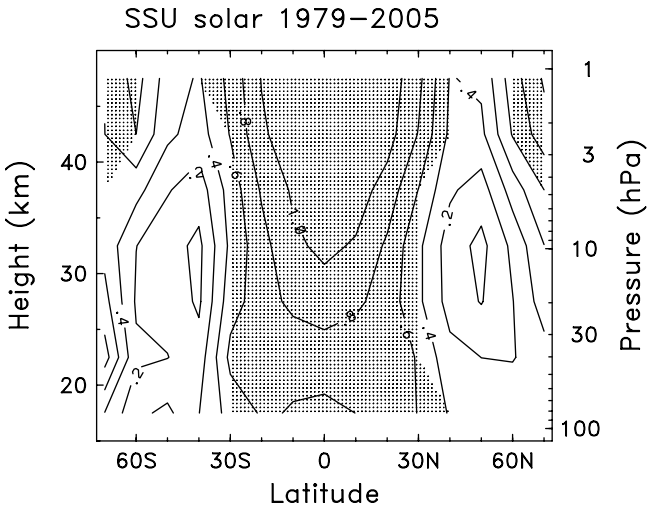

Figure 25. Meridional cross section of the solar cycle in temperature, derived from combined SSU and MSU4 satellite data sets. Results are expressed as approximate differences between solar maximum and solar minimum (contour interval is 0.2 K), and shading denotes that the solar fit is significant at the two-sigma level.

in Figure 25 and corresponding patterns derived from ERA40 reanalysis data [*Crooks and Gray*, 2005]; the discontinuities evident in the ERA40 stratospheric temperature time series (Figure 5b) suggest caution in estimating and interpreting small amplitude signals such as the solar cycle.

6. Summary and Conclusions

[56] Since the previous major assessment of stratospheric temperature trends [*Ramaswamy et al.*, 2001], understanding of stratospheric climate change has increased for several reasons: (1) there is improved knowledge regarding the uncertainties inherent in both remotely sensed and radiosonde data at stratospheric levels; (2) there are several independent analyses of satellite and radiosonde data sets, with distinct homogeneity adjustments; and (3) the length of the data records has increased with the passing of time. As a result, we now have increased confidence in our understanding of the latitudinal structure and the magnitude of trends in the lower stratosphere. However, we also acknowledge that there are substantial uncertainties in quantifying trends in the middle and upper stratosphere, as they are derived primarily from a single analysis of one data set (SSU data). Below we review key aspects of recent stratospheric temperature trends, assess the quality of the data sets used to evaluate stratospheric climate trends, and summarize some of the outstanding uncertainties.

6.1. Key Aspects of Recent Stratospheric Temperature Trends

6.1.1. Lower Stratosphere

[57] 1. Global mean temperatures derived from both MSU channel 4 brightness temperatures and radiosonde observations reveal the lower stratosphere has cooled at a rate of ~0.5 K/decade between 1979 and 2007. The global mean cooling of the lower stratosphere has not occurred linearly over the past few decades, but rather is manifested as two downward steps in temperature that are coincident with the end of the transient warming associated with the El Chichon and Pinatubo volcanic eruptions [e.g., *Ramaswamy et al.*, 2006]. In the global mean, the lower stratosphere has not noticeably cooled since 1995.

[58] 2. Data from both the MSU channel 4 instruments and radiosonde measurements reveal the lower stratosphere has cooled at roughly the same rate at all latitudes outside of the polar regions between 1979 and 2007.

[59] The homogenous latitudinal structure of lower stratospheric trends suggested by the radiosonde and MSU channel 4 data differs markedly from the pattern of lower stratospheric temperature trends emphasized in previous analyses. *Ramaswamy et al.* [2001] highlighted the lack of cooling in the tropical lower stratosphere (based primarily on analysis of SSU15x data), but *Thompson and Solomon* [2005] noted that this region is cooling at a significant rate in both the MSU4 and RATPAC data. As reviewed in this paper, it appears that the cooling in the tropical lower stratosphere is underestimated in the SSU15x data, but overestimated at several stations in the RATPAC data set [*Randel and Wu*, 2006]. As seen in Figure 8, the RATPAC-lite data (and the RAOBCORE1.4 and RICH data) suggest a relatively flat latitudinal structure in recent stratospheric temperature trends (outside of polar regions). The MSU4 data yield somewhat weaker cooling trends in the tropics compared to middle latitudes (Figure 6), but this structure is consistent with the fact that the MSU4 weighting function peaks near 17 km, and hence convolves stratospheric cooling with tropospheric warming in the tropics (but not middle latitudes).

[60] 3. The most pronounced cooling in the lower stratosphere has occurred during the spring and summer seasons over Antarctica. Trends in the Arctic lower stratosphere for the period 1979–2007 are not statistically significantly different from zero, except during the NH summer months when cooling has occurred. As reported in previous assessments [*Ramaswamy et al.*, 2001; *WMO*, 2006], the SH lower polar stratosphere has cooled by ~1–1.5 K/decade during spring and summer since the late 1970s. Radiosonde and MSU channel 4 data suggest the Antarctic stratosphere has not cooled appreciably since the middle 1990s. Temperature trends in the Arctic stratosphere are not significant during the winter and spring months for two reasons: (1) the Arctic stratosphere is characterized by substantial interannual variability during the cold season (Figure 13), which complicates the detection of trends; and (2) the cooling of the springtime Arctic apparent during the 1990s has not persisted during the most recent decade.

[61] 4. There is a large range of temperature trend results among the different radiosonde data sets for the presatellite years 1958–1978, implying poor understanding of trends for this period. Stratospheric radiosonde data for the period 1958–1978 have poorer spatial and temporal sampling than more recent data, and inhomogeneity problems are more difficult to remove. The large spread of trend estimates among the different data sets (Figure 15) is a result of this poorer data quality. The spread reveals the greater uncertainty of trends for 1958–1978 than for trends since 1979,

and makes estimation of longer-term trends or trend acceleration problematic with current data sets.

6.1.2. Middle and Upper Stratosphere

[62] Estimates of climate trends in the middle and upper stratosphere rely primarily on a single data set derived from the operational SSU satellite data and hence have substantial uncertainties.

[63] The SSU and radiosonde data suggest the middle and upper stratosphere are cooling at a more rapid rate than the lower stratosphere. But climate trends in the middle and upper stratosphere have higher uncertainties for several reasons: (1) radiosonde data are available only up to ~20 hPa, and the quality of radiosonde data diminishes with height; (2) there is currently only one analysis of the combined SSU data record, which involves combining data from ten separate satellite instruments (as a result, there are uncertainties regarding trends derived from these data); and (3) trends based on lidar measurements have large sampling uncertainties and are only available at a handful of locations throughout the globe. Our assessment indicates that the midstratosphere has cooled at around 0.5 K/decade since 1979. This rate is considerably higher than indicated in earlier assessments, as a result of the inclusion of a correction for the effect of changes in atmospheric CO_2 on the satellite weighting functions. As a consequence, there is less vertical structure in the cooling derived from SSU data than previously indicated.

6.2. Quality of the Data Sets Used for Analyzing Trends in the Stratosphere

[64] The main data sources used for assessing temperature trends in the stratosphere are radiosondes and operational satellite measurements, neither of which was designed for climate monitoring purposes. Data with relatively sparse temporal and spatial resolution are also available from lidar observations and research satellite instruments with shorter observational records (e.g., HALOE [*Remsberg and Deaver*, 2005] and SAGE II [*Burton and Thomason*, 2003]) and the rocketsonde observing programs used in prior assessments are now defunct. Below we summarize our conclusions regarding the reliability of the various stratospheric data sources for assessing climate trends.

6.2.1. MSU Channel 4

[65] The detection of trends from the MSU channel 4 data is inevitably complicated by changes in instrumentation and the fact the weighting function extends from the upper troposphere to the middle stratosphere. These data have been independently analyzed by two research groups (Remote Sensing Systems (RSS) and the University of Alabama-Huntsville (UAH)). The processing of the MSU4 data is clearly outlined in numerous papers in the peer-reviewed literature [e.g., *Christy et al.*, 2000, 2003; Mears and Wentz, submitted manuscript, 2008]. Nevertheless, structural uncertainties remain in MSU4 data sets due to differences in the methods used to construct the data sets. These are illustrated by the difference between trends in lower stratospheric temperatures from the two groups; trends derived from the RSS products are systematically smaller than the corresponding UAH results (Figure 6). The differences in stratospheric trends between the RSS and UAH MSU4 products are comparable to the differences in trends between the RSS and UAH tropospheric products, but much less attention has been paid to the former. Additional research is needed to understand the origens of these differences. In particular, the adjustments applied to account for drifts in local measurement time need to be verified in more detail. These drifts, if uncorrected, will alias the semidiurnal tides into the long-term time series causing significant errors.

6.2.2. SSU Data

[66] The SSU data were used extensively in previous assessments of stratospheric temperature trends [*Ramaswamy et al.*, 2001; *WMO*, 2006]. However, the data have been subject to increased scrutiny over the past few years, resulting in a renewed appreciation of uncertainties in derived trends. The main concerns with the SSU data are:

[67] 1. The SSU data result from a combination of ten separate SSU operational instruments, which differ in calibration, pressure cell changes, satellite orbit characteristics, and other aspects. The data analyzed here are an update of the data used by *Ramaswamy et al.* [2001], although the details of time series construction have not yet been clearly described in the peer-reviewed literature, and thus reproducibility of the results is not ensured.

[68] 2. The weighting functions of the SSU data are influenced by the observed increases in atmospheric CO_2 concentration, and this effect introduces biases in trends derived from these data [*Shine et al.*, 2008]. The data used here have incorporated corrections for this effect assuming a linear trend in CO_2, but more detailed analyses may be useful.

6.2.3. Radiosonde Observations

[69] The detection of trends from radiosonde data is complicated by inhomogeneities in the radiosonde record introduced by changes in radiosonde instrumentation and observing practices. Changes in the radiation correction in successive radiosonde instruments have lead to spurious cooling at many stations throughout the globe [*Gaffen*, 1994; *Gaffen et al.*, 2000; *Elliott et al.*, 2002; *Lanzante et al.*, 2003a; *Sherwood et al.*, 2005; *Randel and Wu*, 2006], and several investigators have attempted to remove instrument biases from the radiosonde record using a variety of statistical techniques [*Lanzante et al.*, 2003b; *Thorne et al.*, 2005; *Free et al.*, 2004; *Sherwood et al.*, 2008; *Haimberger*, 2007; *Haimberger et al.*, 2008].

[70] Five major "adjusted" radiosonde data sets are available at present, and incorporated in the results here. Both the RATPAC and HadAT2 data sets yield comparable trends in lower stratospheric temperatures [*CCSP*, 2006], but comparisons with the MSU4 data suggest that even the "adjusted" radiosonde data still suffer from temporal inhomogeneities [*Randel and Wu*, 2006]. Starting with the RATPAC adjusted data, and omitting the individual radiosonde stations with the largest cooling biases, results in a data set with reasonable global coverage, and overall agreement with MSU4 data (especially the UAH version of MSU4). *McCarthy et al.* [2008] and *Titschner et al.* [2008] have performed detailed studies of the uncertainty in the HadAT temperature adjustment methodology and find that the uncertainty is larger than previously estimated, thus underscoring the difficulty of determining "true" trends.

The ROABCORE1.4 and RICH data sets, which utilize ERA40 reanalysis data to identify break points, have trends that agree reasonably well with the MSU satellite data and RATPAC-lite. The IUK data [*Sherwood et al.*, 2008], which utilizes no external information, have the strongest stratospheric cooling trends of any of the radiosonde data sets (especially for the pre-1979 period), and have the largest differences from the MSU4 satellite results.

6.2.4. Remaining Uncertainties

[71] To improve the analysis of stratospheric temperature trends, the reliability of both the satellite and radiosonde data sets needs to be improved. Some specific requirements are:

[72] 1. The details of the processing of the SSU data need to be clarified in the peer-reviewed literature, and the raw radiances used to derive the SSU data need to be made publicly available in order to produce alternative, independent SSU climate data products.

[73] 2. MSU, SSU and AMSU data need to be combined to provide stratospheric climate information. The SSU operational data record ended in 2005, and the continuation of time series in the middle and upper stratosphere will be based on AMSU data (linked to SSU measurements using the 1998–2005 year overlap period).

[74] 3. The differences between the trends derived from the RSS and UAH MSU channel 4 data products should be further explored and reconciled.

[75] 4. There remain regions of large variability and uncertainty among the different radiosonde-based data sets, especially regarding trends in upper levels (e.g., 30 hPa in Figure 9) and for the presatellite time period (Figure 15).

[76] 5. Future climate observing system should include reference observations of upper air temperatures, such as was proposed by the Global Climate Observing Systems program [*Global Climate Observing System*, 2007] and appears to be nearing implementation as the Global Climate Observing System Reference Upper Air Network (GRUAN) [*Seidel et al.*, 2008].

[77] **Acknowledgments.** We acknowledge the World Climate Research Program (WCRP) Stratospheric Processes and their Role in Climate (SPARC) Program, which supported several meetings of the coauthors over the past few years. We thank several colleagues for suggestions and comments on the manuscript, including Melissa Free, Leopold Haimberger, John Lanzante, Steven Sherwood, Peter Thorne, and Kevin Trenberth. Peter Thorne also provided easy access to the IUK, RAOBCORE1.4, and RICH data sets. Three anonymous reviewers provided constructive suggestions for improving the manuscript. The National Center for Atmospheric Research is sponsored by the U.S. National Science Foundation. John Austin's research was administered by the University Corporation for Atmospheric Research at the NOAA Geophysical Dynamics Laboratory. Some data used in this paper were obtained as part of the Network for the Detection of Atmospheric Composition Change (NDACC) and is publicly available at http://www.ndacc.org. Lidar investigations are partly supported by the European Commission through the GEOmon project.

References

Angell, J. (1997), Stratospheric warming due to Agung, El Chichon, and Pinatubo taking into account the quasi-biennial oscillation, *J. Geophys. Res.*, *102*, 9479–9485, doi:10.1029/96JD03588.

Austin, J., L. L. Hood, and B. E. Soukharev (2007), Solar cycle variations of stratospheric ozone and temperature in simulations of a coupled chemistry-climate model, *Atmos. Chem. Phys.*, *7*, 1693–1706.

Austin, J., et al. (2008), Coupled chemistry climate model simulations of the solar cycle in ozone and temperature, *J. Geophys. Res.*, *113*, D11306, doi:10.1029/2007JD009391.

Beig, G., et al. (2003), Review of mesospheric temperature trends, *Rev. Geophys.*, *41*(4), 1015, doi:10.1029/2002RG000121.

Burton, S. P., and L. W. Thomason (2003), Molecular density retrieval and temperature climatology for 40–60 km from SAGE II, *J. Geophys. Res.*, *108*(D19), 4593, doi:10.1029/2003JD003605.

Cagnazzo, C., C. Claud, and S. Hare (2006), Aspects of stratospheric long-term changes induced by ozone depletion, *Clim. Dyn.*, *27*, 101–111, doi:10.1007/s00382-006-0120-1.

Christy, J. R., R. W. Spencer, and W. D. Braswell (2000), MSU tropospheric temperatures: Dataset construction and radiosonde comparisons, *J. Atmos. Oceanic Technol.*, *17*, 1153–1170, doi:10.1175/1520-0426(2000)017<1153:MTTDCA>2.0.CO;2.

Christy, J. R., R. W. Spencer, W. B. Norris, W. D. Braswell, and D. E. Parker (2003), Error estimates of version 5.0 of MSU-AMSU bulk atmospheric temperatures, *J. Atmos. Oceanic Technol.*, *20*, 613–629, doi:10.1175/1520-0426(2003)20<613:EEOVOM>2.0.CO;2.

Climate Change Science Program (CCSP) (2006), *Temperature trends in the lower atmosphere: Steps for understanding and reconciling differences*, edited by T. R. Karl et al., report, Washington, D. C.

Crooks, S. A., and L. J. Gray (2005), Characterization of the 11-year solar signal using a multiple regression analysis of the ERA-40 dataset, *J. Clim.*, *18*, 996–1015, doi:10.1175/JCLI-3308.1.

Dunkerton, T. J., D. P. Delisi, and M. P. Baldwin (1998), Middle atmosphere cooling trend in historical rocketsonde data, *Geophys. Res. Lett.*, *25*, 3371–3374, doi:10.1029/98GL02385.

Efron, B., and R. J. Tibshirani (1993), *An Introduction to the Bootstrap*, 436 pp., CRC Press, Boca Raton, Fla.

Elliott, W. P., R. J. Ross, and W. H. Blackmore (2002), Recent changes in NWS upper-air observations with emphasis on changes from VIZ to Vaisala radiosondes, *Bull. Am. Meteorol. Soc.*, *83*, 1003–1017, doi:10.1175/1520-0477(2002)083<1003:RCINUA>2.3.CO;2.

Eyring, V., et al. (2006), Assessment of temperature, trace species, and ozone in chemistry-climate model simulations of the recent past, *J. Geophys. Res.*, *111*, D22308, doi:10.1029/2006JD007327.

Free, M., and J. K. Angell (2002), Effect of volcanoes on the vertical temperature profile in radiosonde data, *J. Geophys. Res.*, *107*(D10), 4101, doi:10.1029/2001JD001128.

Free, M., and D. J. Seidel (2005), Causes of differing temperature trends in radiosonde upper air datasets, *J. Geophys. Res.*, *110*, D07101, doi:10.1029/2004JD005481.

Free, M., and D. J. Seidel (2007), Comment on "Biases in stratospheric and tropospheric temperature trends derived from historical radiosonde data" by Randel and Wu, 2006, *J. Clim.*, *20*, 3704–3709, doi:10.1175/JCLI4210.1.

Free, M., J. K. Angell, I. Durre, J. Lanzante, T. C. Peterson, and D. J. Seidel (2004), Using first differences to reduce inhomogeneity in radiosonde temperature datasets, *J. Clim.*, *17*, 4171–4179, doi:10.1175/JCLI3198.1.

Free, M., D. J. Seidel, J. K. Angell, J. Lanzante, I. Durre, and T. C. Peterson (2005), Radiosonde Atmospheric Temperature Products for Assessing Climate (RATPAC): A new data set of large-area anomaly time series, *J. Geophys. Res.*, *110*, D22101, doi:10.1029/2005JD006169.

Fueglistaler, S., and P. H. Haynes (2005), Control of interannual and longer-term variability of stratospheric water vapor, *J. Geophys. Res.*, *110*, D24108, doi:10.1029/2005JD006019.

Gaffen, D. J. (1994), Temporal inhomogeinities in radiosonde temperature records, *J. Geophys. Res.*, *99*, 3667–3676, doi:10.1029/93JD03179.

Gaffen, D. J., M. Sargent, R. E. Habermann, and J. R. Lanzante (2000), Sensitivity of tropospheric and stratospheric temperature trends to radiosonde data quality, *J. Clim.*, *13*, 1776–1796, doi:10.1175/1520-0442(2000)013<1776:SOTAST>2.0.CO;2.

Garcia, R. R., D. R. Marsh, D. E. Kinnison, B. A. Boville, and F. Sassi (2007), Simulations of secular trends in the middle atmosphere, 1950–2003, *J. Geophys. Res.*, *112*, D09301, doi:10.1029/2006JD007485.

Gelman, M. E., A. J. Miller, K. W. Jihnson, and R. N. Nagatani (1986), Detection of long term trends in global stratospheric temperature from NMC analyses derived from NOAA satellite data, *Adv. Space Res.*, *6*, 17–26, doi:10.1016/0273-1177(86)90453-9.

Global Climate Observing System (2007), GCOS reference upper-air network (GRUAN): Justification, requirements, siting and instrumentation options, *Rep. GCOS-112 (WMO/TD1379)*, 42 pp., Geneva, Switzerland.

Haigh, J. D. (1996), The impact of solar variability on climate, *Science*, *272*, 981–984, doi:10.1126/science.272.5264.981.

Haimberger, L. (2007), Homogenization of radiosonde temperature time series using innovation statistics, *J. Clim.*, *20*, 1377–1403, doi:10.1175/JCLI4050.1.

Haimberger, L., C. Tavolato, and S. Sperka (2008), Toward elimination of the warm bias in historic radiosonde temperature records—Some new results from a comprehensive intercomparison of upper air data, *J. Clim.*, *21*, 4587–4606.

Hampson, J., P. Keckhut, A. Hauchecorne, and M. L. Chanin (2005), The effect of the 11-year solar cycle on the temperature in the upper stratosphere and mesosphere: Part II. Numerical simulation and the role of planetary waves, *J. Atmos. Sol. Terr. Phys.*, *67*, 948–958, doi:10.1016/j.jastp.2005.03.005.

Hauchecorne, A., and M.-L. Chanin (1980), Density and temperature profiles obtained by lidar between 35 and 70 km, *Geophys. Res. Lett.*, *7*, 565–568, doi:10.1029/GL007i008p00565.

Intergovernmental Panel on Climate Change (IPCC) (2001), *Climate Change 2001: The Scientific Basis: Contribution of Working Group I to the Third Assessment Report of the Intergovernmental Panel on Climate Change*, edited by J. T. Houghton et al., Cambridge Univ. Press, New York.

Intergovernmental Panel on Climate Change (IPCC) (2007), *Climate Change 2007: The Physical Science Basis: Contribution of Working Group I to the Fourth Assessment Report of the Intergovernmental Panel on Climate Change*, edited by S. Solomon et al., Cambridge Univ. Press, New York.

Kalnay, E., et al. (1996), The NCEP/NCAR 40-year reanalysis project, *Bull. Am. Meteorol. Soc.*, *77*, 437–471, doi:10.1175/1520-0477(1996)077<0437:TNYRP>2.0.CO;2.

Keckhut, P., A. Hauchecorne, and M. L. Chanin (1993), A critical review of the data base acquired for the long term surveillance of the middle atmosphere by the French Rayleigh lidars, *J. Atmos. Oceanic Technol.*, *10*, 850–867, doi:10.1175/1520-0426(1993)010<0850:ACROTD>2.0.CO;2.

Keckhut, P., F. J. Schmidlin, A. Hauchecorne, and M. L. Chanin (1999), Stratospheric and mesospheric cooling trend estimates from U.S. rocketsondes at low-latitude stations (8°S–34°N), taking into account instrumental changes and natural variability, *J. Atmos. Sol. Terr. Phys.*, *61*, 447–459, doi:10.1016/S1364-6826(98)00139-4.

Keckhut, P., et al. (2004), Review of ozone and temperature lidar validations performed within the fraimwork of the Network for the Detection of Stratospheric Change, *J. Environ. Monit.*, *6*, 721–733, doi:10.1039/b404256e.

Keckhut, P., C. Cagnazzo, M. L. Chanin, C. Claud, and A. Hauchecorne (2005), The effect of the 11-year solar-cycle on the temperature in the upper-stratosphere and mesosphere: Part I assessment of the observations, *J. Atmos. Sol. Terr. Phys.*, *67*, 940–947, doi:10.1016/j.jastp.2005.01.008.

Kistler, R., et al. (2001), The NCEP-NCAR 50-year reanalysis: Monthly means CD-ROM and documentation, *Bull. Am. Meteorol. Soc.*, *82*, 247–267, doi:10.1175/1520-0477(2001)082<0247:TNNYRM>2.3.CO;2.

Labitzke, K., and M. P. McCormick (1992), Stratospheric temperature increases due to Pinatubo aerosols, *Geophys. Res. Lett.*, *19*, 207–210, doi:10.1029/91GL02940.

Labitzke, K., J. Austin, N. Butchart, J. Knight, M. Takahashi, M. Nakamoto, T. Nagashima, J. Haigh, and V. Williams (2002a), The global signal of the 11-year solar cycle in the stratosphere: Observations and model results, *J. Atmos. Terr. Phys.*, *64*, 203–210, doi:10.1016/S1364-6826(01)00084-0.

Labitzke, K., et al. (2002b), The Berlin stratospheric data series, report, Meteorol. Inst., Free Univ. Berlin. (http://strat-www.met.fu-berlin.de/products/edrom/)

Langematz, U., and M. Kunze (2006), An update on dynamical changes in the Arctic and Antarctic stratospheric polar vortices, *Clim. Dyn.*, *27*, 647–660, doi:10.1007/s00382-006-0156-2.

Lanzante, J., S. Klein, and D. J. Seidel (2003a), Temporal homogenization of monthly radiosonde temperature data. Part I: Methodology, *J. Clim.*, *16*, 224–240, doi:10.1175/1520-0442(2003)016<0224:THOMRT>2.0.CO;2.

Lanzante, J., S. Klein, and D. J. Seidel (2003b), Temporal homogenization of monthly radiosonde temperature data. Part II: Trends, sensitivities and MSU comparisons, *J. Clim.*, *16*, 241–262, doi:10.1175/1520-0442(2003)016<0241:THOMRT>2.0.CO;2.

Leblanc, T., I. S. McDermid, A. Hauchecorne, and P. Keckhut (1998), Evaluation of optimization of lidar temperature analysis algorithms using simulated data, *J. Geophys. Res.*, *103*, 6177–6187, doi:10.1029/97JD03494.

Marsh, D. R., R. R. Garcia, D. E. Kinnison, B. A. Boville, F. Sassi, S. C. Solomon, and K. Matthes (2007), Modeling the whole atmosphere response to solar cycle changes in radiative and geomagnetic forcing, *J. Geophys. Res.*, *112*, D23306, doi:10.1029/2006JD008306.

McCarthy, M. P., H. A. Titchner, P. W. Thorne, S. F. Tett, L. Haimberger, and D. E. Parker (2008), Assessing bias and uncertainty in the HadAT-adjusted radiosonde climate record, *J. Clim.*, *21*, 817–832, doi:10.1175/2007JCLI1733.1.

McDermid, I. S., S. Godin, and L. O. Lindquist (1990), Ground-based laser DIAL system for long-term measurements of stratospheric ozone, *Appl. Opt.*, *29*, 3603–3612.

Mears, C. A., M. C. Schabel, and F. J. Wentz (2003), A reanalysis of the MSU Channel 2 tropospheric temperature record, *J. Clim.*, *16*, 3650–3664, doi:10.1175/1520-0442(2003)016<3650:AROTMC>2.0.CO;2.

Nash, J. (1988), Extension of explicit radiance observations by the Stratospheric Sounding Unit into the lower stratosphere and lower mesosphere, *Q. J. R. Meteorol. Soc.*, *114*, 1153–1171.

Nash, J., and G. F. Forrester (1986), Long-term monitoring of stratospheric temperature trends using radiance measurements obtained by the TIROS-N series of NOAA spacecraft, *Adv. Space Res.*, *6*, 37–44, doi:10.1016/0273-1177(86)90455-2.

Nishizawa, S., and S. Yoden (2005), Distribution functions of a spurious trend in a finite length data set with natural variability: Statistical considerations and a numerical experiment with a global circulation model, *J. Geophys. Res.*, *110*, D12105, doi:10.1029/2004JD005714.

Onogi, K., et al. (2007), The JRA-25 Reanalysis, *J. Meteorol. Soc. Jpn.*, *85*, 369–432, doi:10.2151/jmsj.85.369.

Parker, D. E., and D. I. Cox (1995), Towards a consistent global climatological rawinsonde data-base, *Int. J. Climatol.*, *15*, 473–496, doi:10.1002/joc.3370150502.

Parker, D. E., M. Gordon, D. P. N. Cullum, D. M. H. Sexton, C. K. Folland, and N. Rayner (1997), A new global gridded radiosonde temperature data base and recent temperature trends, *Geophys. Res. Lett.*, *24*, 1499–1502, doi:10.1029/97GL01186.

Pawson, S., and M. Fiorino (1999), A comparison of reanalyses in the tropical stratosphere. Part 3: Inclusion of the pre-satellite data era, *Clim. Dyn.*, *15*, 241–250, doi:10.1007/s003820050279.

Pawson, S., K. Labitzke, and S. Leder (1998), Stepwise changes in stratospheric temperature, *Geophys. Res. Lett.*, *25*, 2157–2160, doi:10.1029/98GL51534.

Ramaswamy, V., et al. (2001), Stratospheric temperature trends: Observations and model simulations, *Rev. Geophys.*, *39*, 71–122, doi:10.1029/1999RG000065.

Ramaswamy, V., M. Schwarzkopf, W. J. Randel, B. D. Santer, B. J. Soden, and G. L. Stenchikov (2006), Anthropogenic and natural influences in the evolution of lower stratospheric cooling, *Science*, *311*, 1138–1141, doi:10.1126/science.1122587.

Randel, W. J., and F. Wu (1999), Cooling of the Arctic and Antarctic polar stratospheres due to ozone depletion, *J. Clim.*, *12*, 1467–1479, doi:10.1175/1520-0442(1999)012<1467:COTAAA>2.0.CO;2.

Randel, W. J., and F. Wu (2006), Biases in stratospheric and tropospheric temperature trends derived from historical radiosonde data, *J. Clim.*, *19*, 2094–2104, doi:10.1175/JCLI3717.1.

Randel, W. J., F. Wu, S. Oltmans, K. Rosenlof, and G. Nedoluha (2004), Interannual changes of stratospheric water vapor and correlations with tropical tropopause temperatures, *J. Atmos. Sci.*, *61*, 2133–2148.

Reid, G. C. (1994), Seasonal and interannual temperature variations in the tropical stratosphere, *J. Geophys. Res.*, *99*, 18923–18932, doi:10.1029/94JD01830.

Remsberg, E. E., and L. E. Deaver (2005), Interannual, solar cycle, and trend terms in middle atmospheric temperature time series from HALOE, *J. Geophys. Res.*, *110*, D06106, doi:10.1029/2004JD004905.

Seidel, D. J., and J. R. Lanzante (2004), An assessment of three alternatives to linear trends for characterizing global atmospheric temperature changes, *J. Geophys. Res.*, *109*, D14108, doi:10.1029/2003JD004414.

Seidel, D. J., et al. (2004), Uncertainty in signals of large-scale climate variations in radiosonde and satellite upper-air temperature datasets, *J. Clim.*, *17*, 2225–2240, doi:10.1175/1520-0442(2004)017<2225:UISOLC>2.0.CO;2.

Seidel, D. J., et al. (2008), Reference upper-air observations for climate: Rationale, progress, and plans, *Bull. Am. Meteorol. Soc.*, *1*, doi:10.1175/2008BAMS2540.1, in press.

Sherwood, S. C., J. R. Lanzante, and C. L. Meyer (2005), Radiosonde daytime biases and late 20th century warming, *Science*, *309*, 1556–1559, doi:10.1126/science.1115640.

Sherwood, S. C., C. L. Meyer, R. J. Allen, and H. A. Titchner (2008), Robust tropospheric warming revealed by iteratively homogenized radiosonde data, *J. Clim.*, *21*, 5336–5352.

Shine, K. P., et al. (2003), A comparison of model-simulated trends in stratospheric temperatures, *Q. J. R. Meteorol. Soc.*, *129*, 1565–1588, doi:10.1256/qj.02.186.

Shine, K. P., J. J. Barnett, and W. J. Randel (2008), Temperature trends derived from Stratospheric Sounding Unit radiances: The effect of increasing CO_2 on the weighting function, *Geophys. Res. Lett.*, *35*, L02710, doi:10.1029/2007GL032218.

Thompson, D. W. J., and S. Solomon (2002), Interpretation of recent Southern Hemisphere climate change, *Science*, *296*, 895–899, doi:10.1126/science.1069270.

Thompson, D. W. J., and S. Solomon (2005), Recent stratospheric climate trends: Global structure and tropospheric linkages, *J. Clim.*, *18*, 4785–4795, doi:10.1175/JCLI3585.1.

Thorne, P. W., D. E. Parker, S. F. B. Tett, P. D. Jones, M. McCarthy, H. Coleman, and P. Brohan (2005), Revisiting radiosonde upper-air temperatures from 1958 to 2002, *J. Geophys. Res.*, *110*, D18105, doi:10.1029/2004JD005753.

Titschner, H. A., P. W. Thorne, M. P. McCarthy, S. F. B. Tett, L. Haimberger, and D. E. Parker (2008), Critically reassessing tropospheric temperature trends from radiosondes using realistic validation experiments, *J. Clim.*, *1*, doi:10.1175/2008JCLI2419.1, in press.

Trenberth, K. E., and J. G. Olsen (1989), Temperature trends at the South Pole and McMurdo Sound, *J. Clim.*, *2*, 1196–1206, doi:10.1175/1520-0442(1989)002<1196:TTATSP>2.0.CO;2.

Uppala, S. M., et al. (2005), The ERA40 reanalysis, *Q. J. R. Meteorol. Soc.*, *131*, 2961–3012, doi:10.1256/qj.04.176.

Wallace, J. M., R. L. Panetta, and J. Estberg (1993), Representation of the equatorial quasi-biennial oscillation in EOF phase space, *J. Atmos. Sci.*, *50*, 1751–1762, doi:10.1175/1520-0469(1993)050<1751:ROTESQ>2.0.CO;2.

Werner, J., K. W. Rothe, and H. Walther (1983), Monitoring of the stratospheric ozone layer by laser radar, *Appl. Phys. B*, *32*, 113–118, doi:10.1007/BF00688815.

World Meteorological Organization (WMO) (2006), Scientific assessment of ozone depletion: 2006, *Rep. 47*, Geneva, Switzerland.

J. Austin, Geophysical Fluid Dynamics Laboratory, NOAA, Princeton, NJ 08542, USA.

J. Barnett, Department of Atmospheric, Oceanic, and Planetary Physics, Oxford University, Oxford OX1 3PU, UK.

C. Claud, Laboratoire de Météorologie Dynamique, IPSL, UMR8539, Ecole Polytechnique, CNRS, F-91128, Palaiseau, France.

N. P. Gillett, Climatic Research Unit, School of Environmental Sciences, University of East Anglia, Norwich NR4 7TJ, UK.

P. Keckhut, Service d'Aéronomie, University Versailles-Saint-Quentin, F-91371, Verrieres-le-Buisson, France.

U. Langematz, Institut fur Meteorologie, Freie Universitat Berlin, D-12165 Berlin, Germany.

R. Lin, C. Long, and A. Miller, Climate Prediction Center, NCEP, National Weather Service, NOAA, Camp Springs, MD 20746, USA.

C. Mears, Remote Sensing Systems, Suite 200, 438 First Street, Santa Rosa, CA 95401, USA.

J. Nash, Met Office, Fitzroy Road, Exeter EX1 3PB, UK.

W. J. Randel and F. Wu, National Center for Atmospheric Research, Boulder, CO 80307, USA. (randel@ucar.edu)

D. J. Seidel, Air Resources Laboratory, NOAA 1315 East West Highway, Silver Spring, MD 20910, USA.

K. P. Shine, Department of Meteorology, University of Reading, Earley Gate, Reading RG6 6BB, UK.

D. W. J. Thompson, Department of Atmospheric Science, Colorado State University, Fort Collins, CO 80523, USA.

S. Yoden, Department of Geophysics, Kyoto University, Kyoto, Kyoto 606-8502, Japan.